patients (13). Thus, drug sensitivity appears to be one of the major determinants of the prognosis of advanced HCC patients treated with chemotherapy. Therefore, a hallmark of successful treatment would be the identification of useful biomarkers for determining the survival benefits offered by each treatment strategy.

In this study, we investigated the gene expression profiles of HCCs using serial analysis of gene expression (SAGE) to identify novel molecular markers or targets for the treatment of HCC (14–18). Here, we identified the upregulation of the *DUT* gene that encodes dUTP pyrophosphatase (dUTPase) in HCC. Markedly, HCC with a high nuclear dUTPase expression correlated with a poorly differentiated morphology and a poor prognosis. *DUT* gene knockdown not only suppressed cell proliferation but also sensitized HuH7 cells to low-dose 5-FU.

Materials and methods

Samples

All HCC tissues, adjacent non-cancerous liver tissues and normal liver tissues were obtained from 110 patients undergoing a hepatectomy between 1997 and 2006 in Kanazawa University Hospital, Kanazawa, Japan. Five normal liver tissue samples were obtained from patients undergoing surgical resection of the liver for the treatment of metastatic colon cancer. These samples were snap-frozen in liquid nitrogen immediately after resection. One hundred and five HCC and surrounding non-cancerous liver samples were obtained from patients undergoing surgical resection of the liver for HCC treatment, and part of these samples were used for the recent study (19). Three HCC and adjacent non-cancerous liver tissue samples were snap-frozen in liquid nitrogen and later used for SAGE. Twenty HCC tissues and their corresponding non-cancerous liver tissues were also snap-frozen and later used for real-time reverse transcription-polymerase chain reaction (RT-PCR) analysis, as described previously (19). Eighty-two additional HCC samples were formalin-fixed, paraffin-embedded and used for immunohistochemistry (IHC). HCC and adjacent non-cancerous liver tissues were histologically characterized, as reported elsewhere (19).

All strategies used for gene expression analysis as well as tissue acquisition processes were approved by the Ethics Committee and the Institutional Review Board of Kanazawa University Hospital. All procedures and risks were explained verbally to each patient, who then provided written informed consent.

Serial analysis of gene expression

Total RNA was purified from each homogenized tissue sample using a ToTally RNA extraction kit (Ambion Inc., Austin, TX, USA), and polyadenylated RNA was isolated using a MicroPoly (A) Pure kit (Ambion). A total of 2.5 μg of mRNA per sample was analysed by SAGE (20, 21). SAGE libraries were randomly sequenced at the Genomic Research Center (Shimadzu-Biotechnology, Kyoto, Japan), and the sequence files were analysed with SAGE 2000 software. The size of each SAGE library was normalized to 300 000 transcripts per library, and the abundance of transcripts was compared with SAGE 2000 software. Monte Carlo simulation was used for selecting genes whose expression levels were significantly different between the two libraries (22). Each SAGE tag was annotated using a gene-mapping website SAGE Genie database (http://cgap.nci.nih.gov/SAGE/) and the Source database (http://smd.stanford.edu/cgi-bin/source/sourceSearch), as described previously (23).

Quantitative reverse transcription-polymerase chain reaction

A 1 μg aliquot of each total RNA was reverse-transcribed using SuperScript II reverse-transcriptase (Invitrogen, Carlsbad, CA, USA). Real-time RT-PCR analysis was performed using the ABI PRISM 7700 sequence detection system (Applied Biosystems, Foster City, CA, USA). Using the standard curve method, quantitative PCR was performed in duplicate for each sample–primer set. Each sample was normalized relative to β actin. The assay IDs used were Hs00798995_s1 for dUTPase and Hs99999903_m1 for β actin.

RNA interference targeting *DUT*

Small interfering RNAs (siRNAs) targeting *DUT* or control (scrambled sequence) were synthesized by Dharmacon (Dharmacon Research Inc., Lafayette, CO, USA). The target sequences of *DUT* are 5′-AAGUUGU GAAAACGGACAUUC-3′ (DUT1) and 5′-CGGACAUU CAGAUAGCGCUTT-3′ (DUT2). Lipofectamine 2000™ reagent (Invitrogen) was used for transfection according to the manufacturer's instructions.

Cell proliferation assay, soft agar assay and matrigel invasion assay

Cell proliferation assays were performed using a Cell Titer96 Aqueous kit in quintuplicate (Promega, Madison, WI, USA). For the soft agar assay, 1×10^4 cells were suspended in 2 ml of 0.36% agar with growth medium and added in each well of a six-well plate containing a base layer of 0.72% agar. The plates were incubated at 37 °C in a 5% CO_2 incubator for 2 weeks. Matrigel invasion assays were performed using BD BioCoat™ Matrigel Matrix Cell Culture Inserts and Control Inserts (BD Biosciences, San Jose, CA, USA), as described in the manufacturer's instruction. 5-FU was obtained from Kyowa Kirin (Kyowa Kirin, Tokyo, Japan). All experiments were repeated at least twice.

Immunohistochemistry

Mouse monoclonal anti-dUTPase antibody M01 (Abnova Corporation, Taipei, Taiwan) and mouse antiproliferating

cell nuclear antigen (PCNA) monoclonal antibody PC10 (Calbiochem, San Diego, CA, USA) were used to evaluate the immunoreactivity of HCC and adjacent non-cancerous liver samples using a Dako EnVision+™ kit (Dako, Carpinteria, CA, USA), according to the manufacturer's instruction. Immunoreactivity was evaluated by determining the percentage of cells expressing dUTPase in the examined fields, graded as low (0–50%) or high (> 50%). The PCNA index was evaluated as described previously (19).

Statistical analysis

Student's *t*-test was used to determine the statistical significance of the differences in cell viability between the two groups. The Mann–Whitney *U*-test was used for the analysis of gene expression between chronic liver disease (CLD) and HCC tissues. The χ^2-test was used to evaluate the correlation between clinicopathological characteristics and dUTPase expression status. Univariate and multivariate Cox proportional hazards regression analysis was used to evaluate the association of dUTPase expression and clinicopathological parameters with patient outcome. All statistical analyses were performed using SPSS software (SPSS software package; SPSS Inc., Chicago, IL, USA) and GRAPHPAD PRISM software (GraphPad Software Inc., La Jolla, CA, USA).

Results

Gene expression profiling identified the overexpression of *DUT* in hepatocellular carcinoma

To overcome the considerable individual variability of transcriptomic characteristics, we constructed a SAGE library of normal human liver using RNAs derived from five normal liver tissues. In addition, we constructed two SAGE libraries derived from three HCC tissues or corresponding non-cancerous liver tissues from patients who developed HCC with a history of chronic hepatitis C. We detected a total of 226 267 tags corresponding to 45 746 unique tags from these SAGE libraries (supporting information Table S1). After excluding the tags detected only once in each library, we selected 15 333 reliable unique transcripts expressed in at least one of the SAGE libraries to avoid contamination of tags derived from sequence errors. Then, we annotated these transcripts using SAGE Genie database and the Source database to identify the potential subcellular localization of transcripts categorized into eight groups in each SAGE library.

The number of nuclear component-related transcripts was increased in the HCC library compared with the normal liver and non-cancerous liver libraries, whereas the other cellular component-related transcripts did not show this tendency (supporting information Fig. S1). Because nuclear component-related genes may closely correlate with cancer cell proliferation and chemosensitivity (24), we further investigated the expression of nuclear component-related tags in each library, and identified 10 transcripts associated with nucleotide/nucleoside metabolism that are overexpressed in HCC (Table 1). Using Monte Carlo simulation, we evaluated the significance of differentially expressed transcripts in HCC and corresponding CLD libraries or in HCC and normal liver libraries. We identified a *DUT* gene encoding dUTPase (dUTPase) whose expression was significantly altered ($P = 0.01$). We also identified a *TS* gene encoding thymidylate synthase in the list, but the difference did not reach statistical significance.

dUTPase is a phosphatase known to maintain a dUMP pool by catalysing the hydrolysis of dUTP to dUMP, and thus provides a substrate of thymidylate synthase. Its role in HCC is unknown; therefore, we examined *DUT* expression in 20 independent HCC and corresponding non-cancerous liver tissues, and identified significant overexpression of *DUT* in HCC tissue ($P = 0.0015$) (Fig. 1A). Moreover, we detected more than a two-fold increase in *DUT* expression in 70% of HBV-related and HCV-related HCC cases (14 of 20 HCCs) compared with the non-cancerous liver tissues (Fig. 1B). We further examined the expression of *DUT* in 238 HCC tissues compared with the non-cancerous liver tissues using publicly available microarray data (GSE5975) (Fig. S2). Consistent with the SAGE data, *DUT* was overexpressed more than two-fold in 121 of 238 HCC tissues (median: 2.03), whereas *TS* was overexpressed more than two-fold in 54 of 238 HCC tissues (median: 1.41) compared with the non-cancerous liver tissues.

Pivotal role of dUTP pyrophosphatase expression in cell proliferation in hepatocellular carcinoma cell lines

In general, cancer gene signatures discovered by comparison between tumour and non-tumour tissues are more likely to reflect the differences in the control of cell proliferation and growth (25). Accordingly, we investigated the function of dUTPase in cell proliferation in HuH7 cells by *DUT* gene knockdown. *DUT* expression was decreased by 60–70% following the transfection of the siRNA constructs specifically targeting *DUT* 48 h after transfection (DUT1 in Fig. 2A and DUT2 in Fig. S3A), and cell growth was significantly inhibited compared with the control 72 h after transfection (Fig. 2B and Fig. S3B). Anchorage-independent cell growth was also significantly impaired by *DUT* gene knockdown 14 days after transfection (Fig. 2C). Furthermore, *DUT* gene knockdown decreased the numbers of both migrating and invading cells 72 h after transfection (Fig. 2D and E).

dUTPase is known to be associated with thymidylate synthesis (26), and thus we evaluated the effects of 5-FU, a thymidylate synthase inhibitor, on dUTPase expression in HCC cell lines *in vitro*. When we treated HuH7 cells with low-dose 5-FU (0.25 mg/ml), we could not detect any growth-inhibitory effects (Fig. 2F). Based on this condition, we evaluated the effect of *DUT* gene knockdown on 5-FU sensitivity 72 h after transfection.

Table 1. Genes associated with nucleic acid metabolism overexpressed in hepatocellular carcinoma

Tag sequence	Normal liver	Non-cancerous liver	HCC	Fold*	Gene	*P*-value†
CAGCTCCGCT	0	2	11	5.5	dUTP pyrophosphatase	0.010
AAAGGATAAT	0	0	3	> 3	General transcription factor II H, polypeptide 2	0.127
ACGGTCCAGG	0	0	3	> 3	Cytidine deaminase	0.127
ATGTAGAGTG	0	0	3	> 3	Thymidylate synthase	0.127
TGGGGATTAC	1	0	3	> 3	Zinc ribbon domain containing, 1	0.127
CACCCTGTAC	2	2	6	3	Solute carrier family 29	0.147
GAACGCCTAA	1	1	3	3	Dihydropyrimidinase-like 2	0.308
GCGCTGGTAC	0	1	3	3	2′-5′-oligoadenylate synthetase 3	0.308
CTTAGTGCAA	0	2	4	2	3′-phosphoadenosine 5′-phosphosulphate synthase 2	0.335
TTGTTACATC	0	2	3	1.5	Phosphoribosyl pyrophosphatase synthetase-associated protein 1	0.506

*Fold increase was calculated by dividing the number of tags in HCC by that of tags in non-cancerous liver. To avoid division by 0, a tag value of 1 was used for any tag that was not detectable in one sample.

†Statistical significance of differentially expressed genes between two groups (HCC and non-cancerous liver libraries) was calculated using Monte Carlo simulation.

HCC, hepatocellular carcinoma.

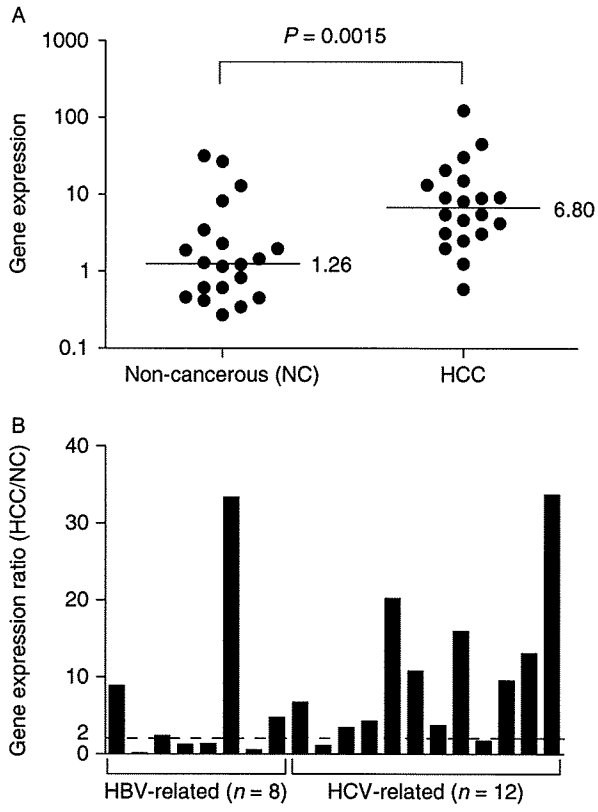

Fig. 1. (A) Quantitative reverse transcription-polymerase chain reaction analysis of *DUT* expression in hepatocellular carcinoma (HCC) and corresponding non-cancerous liver tissues. *DUT* was significantly activated in HCC tissues compared with non-cancerous liver tissues ($P = 0.0015$). A median value in each group is indicated. (B) *DUT* gene expression ratios of HCC and corresponding non-cancerous liver tissues. Fourteen of 20 HCC tissues expressed *DUT* more than two-fold compared with the background non-cancerous liver tissues. HBV, hepatitis B virus; HCV, hepatitis C virus.

Interestingly, *DUT* gene knockdown not only suppressed cell proliferation but also sensitized HuH7 cells to low-dose 5-FU (Fig. 2F and Fig. S3B). These data suggest that dUTPase overexpression in HCC tissues may be associated with enhanced cell proliferation and 5-FU resistance.

Intense dUTP pyrophosphatase expression is correlated with a poor prognosis in hepatocellular carcinoma patients

To characterize the clinicopathological characteristics of dUTPase expression in HCC, we performed IHC using an additional independent HCC cohort. Accordingly, we explored the dUTPase expression in HCC using 82 formalin-fixed paraffin-embedded HCC specimens. All HCC tissues were surgically resected at the Liver Disease Center of Kanazawa University Hospital with full clinical information, and their immunoreactivity to anti-dUTPase antibodies was evaluated by IHC. We noticed that anti-dUTPase antibodies reacted to both nuclear (red arrows) and cytoplasmic (blue arrows) isoforms of dUTPase, as described previously (26) (Fig. 3A and B). We therefore evaluated the nuclear and cytoplasmic expression of dUTPase separately. We stratified HCC tissues and evaluated the dUTPase expression status based on the percentages of dUTPase-positive cells. The frequency of nuclear or cytoplasmic dUTPase-positive cells was highly variable in each HCC tissue, and we defined HCCs with nuclear or cytoplasmic dUTPase expressed in $\geq 50\%$ of tumour cells as nuclear or cytoplasmic dUTPase-high HCC (Fig. 3C). Nuclear dUTPase overexpression was detected in 36.6% (30 of 82), whereas cytoplasmic dUTPase overexpression was detected in 67.1% (55 of 82) of HCC tissues compared with the corresponding non-cancerous liver tissues

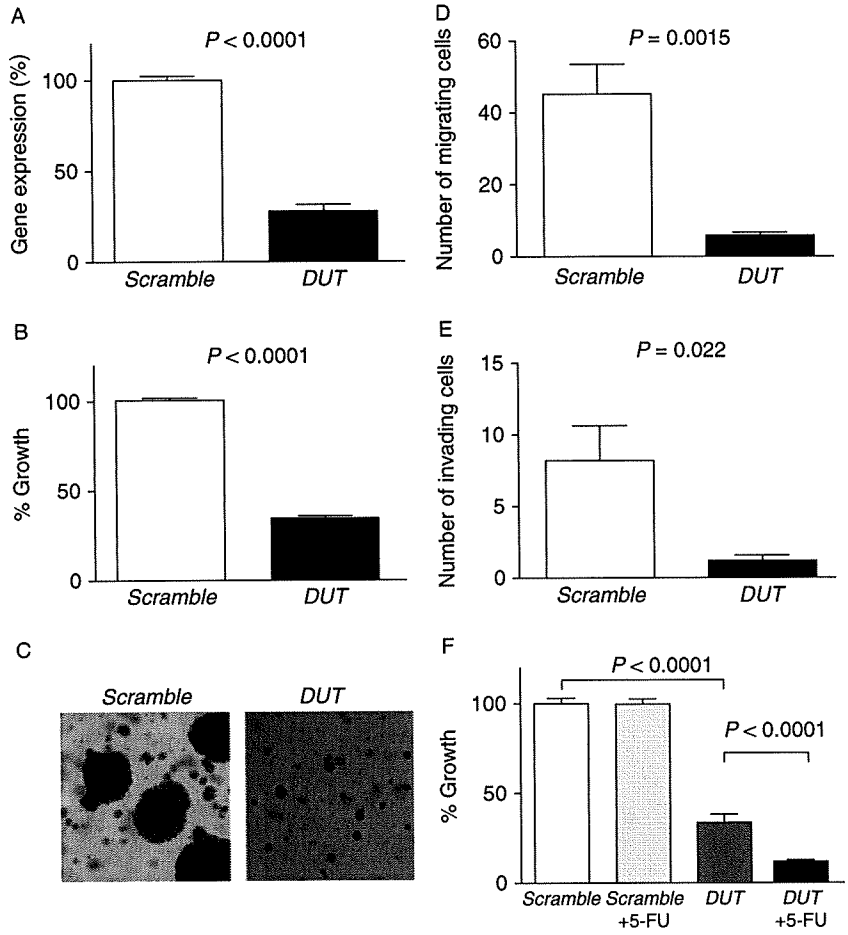

Fig. 2. (A) Transfection of small interfering RNAs targeting *DUT* (DUT1) decreased *DUT* expression compared with the control (scrambled sequence). Gene expression was evaluated in triplicate 72 h after transfection (mean ± SD). (B) *DUT* gene knockdown significantly suppressed cell proliferation ($P < 0.0001$). Cell viability was evaluated in triplicate 72 h after transfection (mean ± SD). (C) Soft agar assay. *DUT* gene knockdown suppressed anchorage-independent cell growth. (D and E) Matrigel invasion assay. *DUT* gene knockdown decreased the numbers of both migrating and invading cells. Experiments were performed in triplicate (mean ± SD). (F) *DUT* gene knockdown sensitized HuH7 cells to low-dose 5-fluorouracil (5-FU) (0.25 μg/ml), which had no effect on the cell proliferation in the control (mean ± SD).

(Table 2). In general, non-cancerous hepatocytes rarely expressed nuclear dUTPase (Fig. 3A).

We investigated the clinicopathological characteristics of nuclear or cytoplasmic dUTPase in low /high HCC cases (Table 2). The expression status of nuclear dUTPase showed no correlation with age, gender, virus, presence of cirrhosis, α-fetoprotein value, tumour size and TNM stages. However, nuclear dUTPase expression was significantly correlated with the histological grades of HCC ($P = 0.0099$), and high frequencies of nuclear dUTPase-positive cells were associated with poorly differentiated cell morphology in the HCC tissue. In contrast, cytoplasmic dUTPase expression was not correlated with the histological grades of HCC ($P = 0.077$). We examined the cell proliferation of these HCC samples by PCNA staining, and PCNA indexes were significantly higher in nuclear dUTPase high HCC than low HCC with statistical significance ($P = 0.01$) (Fig. S4).

We further investigated the prognostic significance of dUTPase expression in HCC. Strikingly, high nuclear dUTPase expression in HCC tissue correlated with a poor survival outcome compared with low nuclear dUTPase expression ($P = 0.0036$), whereas high cytoplasmic dUTPase expression had little effects when evaluated by recurrence-free survival (Fig. 3D). Furthermore, univariate Cox regression analysis showed a significant correlation between high nuclear dUTPase expression and a high risk of mortality (HR, 2.47; 95% CI, 1.08–5.66; $P = 0.032$; Table 3). By multivariate Cox regression analysis, TNM stage (HR, 2.75; 95% CI, 1.11–6.79; $P = 0.027$) and nuclear dUTPase (HR, 2.61; 95% CI, 1.13–6.05; $P = 0.024$) were independent prognostic factors associated with a high risk of mortality, and other clinicopathological features did not add independent prognostic information. These data indicate a significant correlation between the malignant potential of

Liver International (2009)

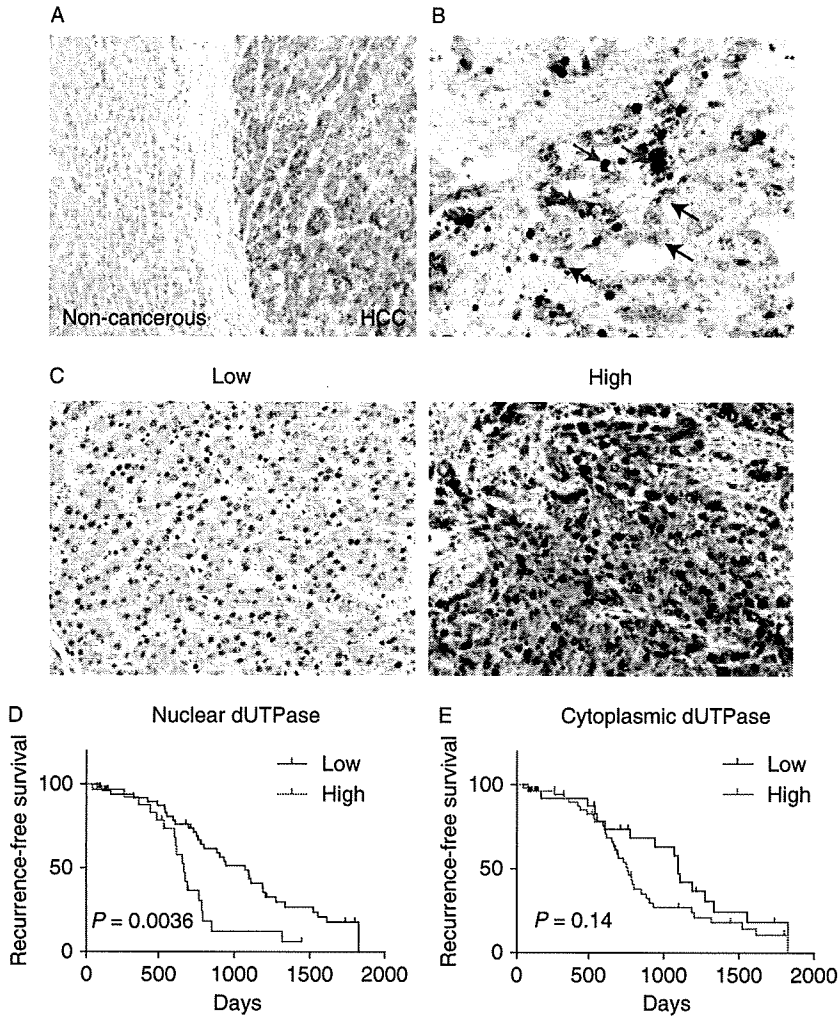

Fig. 3. Immunohistochemistry analysis of dUTP pyrophosphatase (dUTPase) expression in hepatocellular carcinoma (HCC). (A) A representative photomicrograph of dUTPase staining in an HCC and adjacent non-cancerous liver tissue. (B) A representative photomicrograph of dUTPase staining in an HCC. Both nuclear (red arrows) and cytoplasmic (blue arrows) forms of dUTPase were detected. (C) Representative photomicrographs of HCC tissues with low (0–50%) and high (≥50%) frequencies of nuclear and cytoplasmic dUTPase-positive cells. (D and E) Kaplan–Meier survival analysis of HCC tissues with nuclear (D) or cytoplasmic (E) dUTPase expression. High percentages of nuclear dUTPase-positive tumour cells significantly correlated with poor clinical outcome in recurrence-free survival.

HCC and nuclear dUTPase expression, implicating the potential effectiveness of nuclear dUTPase level as a biomarker for predicting the survival of HCC patients after surgical resection.

Discussion

Here, using a global gene expression profiling approach (18), we have identified the activation of the nucleotide/nucleoside metabolism-related gene *DUT* (encoding dUTPase) in HCC. Notably, an intense dUTPase expression was detected in a subset of HCC with a poor prognosis. To the best of our knowledge, this is the first report describing the correlation between dUTPase activation and poor survival outcome in HCC patients.

In normal cells, dUTPase is known to catalyse the hydrolysis of dUTP to dUMP in order to maintain the dUMP pool at a certain level for thymidylate synthesis (26). Interestingly, dUTPase mutations in *Escherichia coli* increased dUTP levels, leading to dUTP misincorporation into DNA during replication, which resulted in DNA fragmentation and apoptosis (27). Furthermore, introduction of *E. coli* dUTPase into human tumour cells resulted in the induction of resistance to fluorodeoxyuridine cytotoxicity (28), suggesting a pivotal role of dUTPase in the prevention of DNA damage. Thus, dUTPase activation in the nucleus appears to be critical

Table 2. Clinicopathological characteristics and dUTP pyrophosphatase expression in hepatocellular carcinoma ($n = 82$)

dUTPase expression (nuclear)	Low ($n = 52$)	High ($n = 30$)	*P*-value
Age (< 60 years/≥60 years)	19/33	8/22	0.36
Sex (male/female)	36/16	23/7	0.47
Virus (HBV/HCV/B+C/NBNC)	15/33/1/3	10/20/0/0	0.48
Cirrhosis (yes/no)	33/19	22/8	0.36
AFP (< 20 ng/ml/≥20 ng/ml)	32/20	15/15	0.31
Histological grade*			
I–II	14	3	
II–III	36	20	
III–IV	2	7	0.0099
Tumour size (< 3 cm/≥3 cm)	31/21	19/11	0.74
TNM classification† (I, II/III, IV)	43/9	25/5	0.94
dUTPase expression (cytoplasmic)	Low ($n = 27$)	High ($n = 55$)	*P*-value
Age (< 60 years/≥60 years)	10/17	17/38	0.58
Sex (male/female)	19/8	40/15	0.82
Virus (HBV/HCV/B+C/NBNC)	8/17/1/1	17/36/0/2	0.56
Cirrhosis (yes/no)	17/10	38/17	0.58
AFP (< 20 ng/ml/≥20 ng/ml)	16/11	31/24	0.80
Histological grade*			
I–II	7	10	
II–III	20	36	
III–IV	0	9	0.077
Tumour size (< 3cm/≥3 cm)	17/10	33/22	0.80
TNM classification† (I, II/III, IV)	21/6	47/8	0.39

*Edmondson–Steiner grades.
†UICC TNM classification of liver cancer, 6th edition (2002).
AFP, α-fetoprotein; dUTPase, dUTP pyrophosphatase; HBV, hepatitis B virus; HCV, hepatitis C virus.

Table 3. Cox regression analysis of recurrence-free survival rate relative to dUTP pyrophosphatase expression and clinicopathological parameters ($n = 82$)

	Univariate		Multivariate	
Variables (n)	HR (95% CI)	*P*-value	HR (95% CI)	*P*-value
Child–Pugh				
A	1			
B	1.73 (0.50–5.97)	0.38		
Tumour size				
< 3 cm ($n = 50$)	1			
≥3 cm ($n = 32$)	1.58 (0.69–3.63)	0.28		
TNM stage*				
I, II ($n = 68$)	1		1	
III, IV ($n = 14$)	2.57 (1.05–6.29)	0.039	2.75 (1.11–6.79)	0.027
Serum AFP				
< 20 ng/ml ($n = 49$)	1			
≥20 ng/ml ($n = 38$)	1.54 (0.66–3.56)	0.31		
Microvascular invasion				
No	1			
Yes	1.98 (0.89–4.44)	0.095		
BCLC stage				
A	1			
B/C	2.16 (0.93–5.00)	0.07		
Cytoplasmic dUTPase				
Low ($n = 27$)	1			
High ($n = 55$)	1.15 (0.50–2.62)	0.73		
Nuclear dUTPase				
Low ($n = 52$)	1		1	
High ($n = 30$)	2.47 (1.08–5.66)	0.032	2.61 (1.13–6.05)	0.024

*UICC TNM classification of liver cancer, 6th edition (2002).
AFP, α-fetoprotein; CI, confidence intervals; dUTPase, dUTP pyrophosphatase; HR, hazard ratio.

for preventing DNA damage possibly at the S phase. Specifically, this activation may prevent dUTP misincorporation in various cancers and thus avert DNA damage and apoptosis induction. Indeed, dUTPase activation has recently been reported in colorectal and brain cancer (29, 30), and dUTPase accumulation might correlate with 5-FU-based chemotherapy resistance and poor prognosis in colorectal cancer (26).

If dUTPase activation plays a central role in the development of resistance to thymidylate synthase inhibitors in order to prevent a DNA damage response, dUTPase inhibition may facilitate the eradication of cancer cells by sensitizing these cells to such inhibitors. Indeed, a recent study suggested a drastic sensitization of colon cancer cells to 5-FU by siRNAs-mediated dUTPase suppression (31, 32), which is consistent with our current observation. Because all HCC samples used in this study were surgically resected, we could not evaluate the effect of dUTPase expression on clinical HCC patients' outcome in relation to chemosensitivity to thymidylate synthase inhibitors. Nevertheless, intense nuclear dUTPase expression may be a good biomarker for predicting the response to thymidylate synthase inhibitors, and its usefulness should be further evaluated in the future.

In conclusion, comprehensive gene expression profiling shed new light on the role of dUTPase in HCC. Nuclear dUTPase accumulation is potentially a good biomarker for predicting poor prognosis in HCC patients, and the development of a dUTPase inhibitor may promote the possibility of tumour eradication in HCC patients.

Acknowledgements

The authors would like to thank Ms Masayo Baba and Nami Nishiyama for technical assistance. This research was supported in part by a Grant-in-Aid for Special Purposes from the Ministry of Education, Culture, Sports, Science and Technology, Japan (no. 20599005).

Grant support: Grant-in-Aid for Special Purposes from the Ministry of Education, Culture, Sports, Science and Technology, Japan (no. 20599005).

References

1. Parkin DM, Bray F, Ferlay J, Pisani P. Global cancer statistics, 2002. *CA Cancer J Clin* 2005; **55**: 74–108.
2. El-Serag HB, Rudolph KL. Hepatocellular carcinoma: epidemiology and molecular carcinogenesis. *Gastroenterology* 2007; **132**: 2557–76.
3. Farazi PA, Depinho RA. Hepatocellular carcinoma pathogenesis: from genes to environment. *Nat Rev Cancer* 2006; **6**: 674–87.
4. Roessler S, Budhu A, Wang XW. Future of molecular profiling of human hepatocellular carcinoma. *Future Oncol* 2007; **3**: 429–39.
5. El-Serag HB, Marrero JA, Rudolph L, Reddy KR. Diagnosis and treatment of hepatocellular carcinoma. *Gastroenterology* 2008; **134**: 1752–63.
6. Llovet JM, Bruix J. Novel advancements in the management of hepatocellular carcinoma in 2008. *J Hepatol* 2008; **48**(Suppl. 1): S20–37.
7. Poon RT, Fan ST, Lo CM, Liu CL, Wong J. Long-term survival and pattern of recurrence after resection of small hepatocellular carcinoma in patients with preserved liver function: implications for a strategy of salvage transplantation. *Ann Surg* 2002; **235**: 373–82.
8. Friedman MA. Primary hepatocellular cancer–present results and future prospects. *Int J Radiat Oncol Biol Phys* 1983; **9**: 1841–50.
9. Lin DY, Lin SM, Liaw YF. Non-surgical treatment of hepatocellular carcinoma. *J Gastroenterol Hepatol* 1997; **12**: S319–28.
10. Nagano H, Miyamoto A, Wada H, *et al.* Interferon-alpha and 5-fluorouracil combination therapy after palliative hepatic resection in patients with advanced hepatocellular carcinoma, portal venous tumor thrombus in the major trunk, and multiple nodules. *Cancer* 2007; **110**: 2493–501.
11. Patt YZ, Hassan MM, Lozano RD, *et al.* Phase II trial of systemic continuous fluorouracil and subcutaneous recombinant interferon alfa-2b for treatment of hepatocellular carcinoma. *J Clin Oncol* 2003; **21**: 421–7.
12. Urabe T, Kaneko S, Matsushita E, Unoura M, Kobayashi K. Clinical pilot study of intrahepatic arterial chemotherapy with methotrexate, 5-fluorouracil, cisplatin and subcutaneous interferon-alpha-2b for patients with locally advanced hepatocellular carcinoma. *Oncology* 1998; **55**: 39–47.
13. Obi S, Yoshida H, Toune R, *et al.* Combination therapy of intraarterial 5-fluorouracil and systemic interferon-alpha for advanced hepatocellular carcinoma with portal venous invasion. *Cancer* 2006; **106**: 1990–7.
14. Honda M, Yamashita T, Ueda T, *et al.* Different signaling pathways in the livers of patients with chronic hepatitis B or chronic hepatitis C. *Hepatology* 2006; **44**: 1122–38.
15. Nishino R, Honda M, Yamashita T, *et al.* Identification of novel candidate tumour marker genes for intrahepatic cholangiocarcinoma. *J Hepatol* 2008; **49**: 207–16.
16. Yamashita T, Honda M, Takatori H, *et al.* Genome-wide transcriptome mapping analysis identifies organ-specific gene expression patterns along human chromosomes. *Genomics* 2004; **84**: 867–75.
17. Yamashita T, Kaneko S, Hashimoto S, *et al.* Serial analysis of gene expression in chronic hepatitis C and hepatocellular carcinoma. *Biochem Biophys Res Commun* 2001; **282**: 647–54.
18. Yamashita T, Honda M, Kaneko S. Application of serial analysis of gene expression in cancer research. *Curr Pharm Biotechnol* 2008; **9**: 375–82.
19. Yamashita T, Honda M, Takatori H, *et al.* Activation of lipogenic pathway correlates with cell proliferation and poor prognosis in hepatocellular carcinoma. *J Hepatol* 2009; **50**: 100–10.
20. Velculescu VE, Zhang L, Vogelstein B, Kinzler KW. Serial analysis of gene expression. *Science* 1995; **270**: 484–7.
21. Yamashita T, Hashimoto S, Kaneko S, *et al.* Comprehensive gene expression profile of a normal human liver. *Biochem Biophys Res Commun* 2000; **269**: 110–6.
22. Polyak K, Xia Y, Zweier JL, Kinzler KW, Vogelstein B. A model for p53-induced apoptosis. *Nature* 1997; **389**: 300–5.
23. Misu H, Takamura T, Matsuzawa N, *et al.* Genes involved in oxidative phosphorylation are coordinately upregulated with fasting hyperglycaemia in livers of patients with type 2 diabetes. *Diabetologia* 2007; **50**: 268–77.
24. Longley DB, Harkin DP, Johnston PG. 5-fluorouracil: mechanisms of action and clinical strategies. *Nat Rev Cancer* 2003; **3**: 330–8.
25. Whitfield ML, George LK, Grant GD, Perou CM. Common markers of proliferation. *Nat Rev Cancer* 2006; **6**: 99–106.
26. Ladner RD, Lynch FJ, Groshen S, *et al.* dUTP nucleotidohydrolase isoform expression in normal and neoplastic tissues: association with survival and response to 5-fluorouracil in colorectal cancer. *Cancer Res* 2000; **60**: 3493–503.
27. El-Hajj HH, Zhang H, Weiss B. Lethality of a dut (deoxyuridine triphosphatase) mutation in *Escherichia coli*. *J Bacteriol* 1988; **170**: 1069–75.
28. Canman CE, Radany EH, Parsels LA, *et al.* Induction of resistance to fluorodeoxyuridine cytotoxicity and DNA damage in human tumor cells by expression of *Escherichia coli* deoxyuridinetriphosphatase. *Cancer Res* 1994; **54**: 2296–8.
29. Fleischmann J, Kremmer E, Muller S, *et al.* Expression of deoxyuridine triphosphatase (dUTPase) in colorectal tumours. *Int J Cancer* 1999; **84**: 614–7.
30. Romeike BF, Bockeler A, Kremmer E, *et al.* Immunohistochemical detection of dUTPase in intracranial tumors. *Pathol Res Pract* 2005; **201**: 727–32.
31. Koehler SE, Ladner RD. Small interfering RNA-mediated suppression of dUTPase sensitizes cancer cell lines to thymidylate synthase inhibition. *Mol Pharmacol* 2004; **66**: 620–6.

32. Wilson PM, Fazzone W, Labonte MJ, *et al.* Novel opportunities for thymidylate metabolism as a therapeutic target. *Mol Cancer Ther* 2008; **7**: 3029–37.

Supporting Information

Additional Supporting Information may be found in the online version of this article:

Fig. S1. Subcellular localization of genes detected in each SAGE library.

Fig. S2. Microarray analysis of *DUT* and *TS* gene expression in 238 HCC cases publicly available (GSE5975). *DUT* was overexpressed more than 2-fold in 121 of 238 HCC tissues (median: 2.03), whereas *TS* was overexpressed more than 2-fold in 54 of 238 HCC tissues (median: 1.41) compared with the non-cancerous liver tissues.

Fig. S3. (A) Transfection of siRNAs targeting *DUT* (DUT2) decreased *DUT* expression compared with the control (scrambled sequence). Gene expression was evaluated in triplicates 72 hours after transfection (mean ± SD). (B) *DUT* gene knockdown sensitized HuH7 cells to low-dose 5-FU (0.25 mg/ml) (mean ± SD).

Fig. S4. Nuclear and cytoplasmic dUTPase expression and cell proliferation in HCC. PCNA indexes in nuclear dUTPase-high HCC were higher than those in -low HCC with statistical significance ($P = 0.01$). Cytoplasmic dUTPase expression was not associated with PCNA indexes in HCC.

Table S1. A summary of constructed SAGE libraries.

Please note: Wiley-Blackwell is not responsible for the content or functionality of any supporting materials supplied by the authors. Any queries (other than missing material) should be directed to the corresponding author for the article.

Histological Course of Nonalcoholic Fatty Liver Disease in Japanese Patients

Tight glycemic control, rather than weight reduction, ameliorates liver fibrosis

ERIKA HAMAGUCHI, MD, PHD[1]
TOSHINARI TAKAMURA, MD, PHD[1]
MASARU SAKURAI, MD, PHD[2]
EISHIRO MIZUKOSHI, MD, PHD[3]
YOH ZEN, MD, PHD[4]
YUMIE TAKESHITA, MD, PHD[1]
SEIICHIRO KURITA, MD, PHD[1]
KUNIAKI ARAI, MD, PHD[3]
TATSUYA YAMASHITA, MD, PHD[3]
MOTOKO SASAKI, MD, PHD[5]
YASUNI NAKANUMA, MD, PHD[5]
SHUICHI KANEKO, MD, PHD[3]

OBJECTIVE — The goal of this study was to examine whether metabolic abnormalities are responsible for the histological changes observed in Japanese patients with nonalcoholic fatty liver disease (NAFLD) who have undergone serial liver biopsies.

RESEARCH DESIGN AND METHODS — In total, 39 patients had undergone consecutive liver biopsies. Changes in their clinical data were analyzed, and biopsy specimens were scored histologically for stage.

RESULTS — The median follow-up time was 2.4 years (range 1.0–8.5). Liver fibrosis had improved in 12 patients (30.7%), progressed in 11 patients (28.2%), and remained unchanged in 16 patients (41%). In a Cox proportional hazard model, decrease in A1C and use of insulin were associated with improvement of liver fibrosis independent of age, sex, and BMI. However, ΔA1C was more strongly associated with the improvement of liver fibrosis than use of insulin after adjustment for each other (χ^2; 7.97 vs. 4.58, respectively).

CONCLUSIONS — Tight glycemic control may prevent histological progression in Japanese patients with NAFLD.

Diabetes Care 33:284–286, 2010

Accumulating trans-sectional evidence suggests that the presence of multiple metabolic disorders, including obesity, diabetes, dyslipidemia, hypertension, and ultimately metabolic syndrome, are associated with nonalcoholic fatty liver disease (NAFLD) (1). However, it remains unclear which metabolic abnormalities are responsible for the pathological progression of NAFLD, especially in Japanese patients, who generally are not severely obese compared with Western patients.

We retrospectively compared clinical features with the histological changes in the livers of Japanese patients with NAFLD who had undergone serial liver biopsies.

RESEARCH DESIGN AND METHODS

— We recruited 195 patients with clinically suspected NAFLD who had undergone liver biopsies at Kanazawa University Hospital from 1997 through 2008. For details about the study subjects and the exclusion criteria, see supplementary Fig. 1 in the online appendix, available at http://care.diabetesjournals.org/cgi/content/full/dc09-0148/DC1. Of 178 patients diagnosed histologically as having NAFLD, 39 had undergone serial liver biopsies.

Data collection

Clinical information, including age, sex, body measurements, and prevalence of metabolic abnormalities, was obtained for each patient. Venous blood samples drawn for laboratory testing before the liver biopsies were obtained. All subjects had been administered a 75-g oral glucose tolerance test at baseline and at follow-up.

Liver biopsies

Biopsies were obtained after a thorough clinical evaluation and receipt of signed informed consent from each patient. All biopsies were analyzed twice and at separate times randomly by a single pathologist who was blinded to the clinical information and the order in which the biopsies were obtained. The biopsied tissues were scored for steatosis, stage, and grade as described (2), according to the standard criteria for grading and staging of nonalcoholic steatohepatitis proposed by Brunt et al. (3).

For additional details on subjects, data collection methods, liver pathology, and statistical analyses, see supplementary Methods in the online appendix.

RESULTS

— The basal clinical and biochemical data from 39 patients with NAFLD are described in supplementary Table 1. Prevalence of type 2 diabetes, hypertension, and dyslipidemia were 77, 36, and 64%, respectively. The median follow-up period was 2.4 years (range 1.0–8.5). Medications for diabetes and medication changes during the follow-up period are described in supplementary Table 2. Seventeen patients treated with oral diabetic agents were switched to insulin therapy after the initial biopsy. No patients initiated pioglitazone during follow-up.

From the [1]Department of Disease Control and Homeostasis, Kanazawa University Graduate School of Medical Science, Ishikawa, Japan; the [2]Department of Epidemiology and Public Health, Kanazawa Medical University, Ishikawa, Japan; the [3]Department of Gastroenterology, Kanazawa University Hospital, Ishikawa, Japan; the [4]Division of Pathology, Kanazawa University Hospital, Ishikawa, Japan; and the [5]Department of Human Pathology, Kanazawa University Graduate School of Medical Science, Ishikawa, Japan.
Corresponding author: Toshinari Takamura, ttakamura@m-kanazawa.jp.
Received 8 February 2009 and accepted 20 October 2009. Published ahead of print at http://care.diabetesjournals.org on 30 October 2009. DOI: 10.2337/dc09-0148.

Table 1—*Baseline and follow-up clinical features and gradients of laboratory markers associated with changes in liver fibrosis in 39 patients with NAFLD*

	Baseline				Follow-up			
	Improved	Stable	Progressed	*P*	Improved	Stable	Progressed	*P*
n	12	16	11		12	16	11	—
Simple fatty liver:nonalcoholic steatohepatitis (*n*)	3:9	9:7	10:1		10:2	9:7	6:5	
Age (years)	51.5 (29–66)	48.5 (20–79)	51.5 (29–66)	0.97				
Sex (M:F)	5:7	12:4	5:7	0.17				
BMI (kg/m^2)	27.5 (23.2–34.1)	27.7 (22.5–44.4)	30.9 (23.4–37.7)	0.74	26.9 (22.8–31.2)	29.1 (24.3–44.8)	30.7 (24.1–36.3)	0.13
Aspartate transaminase (IU/l)	70 (11–106)	29 (14–86)	32 (13–83)	0.05	23 (11–28)	26 (15–71)	24 (14–164)	0.20
Alanine transaminase (IU/l)	71 (10–209)	48 (23–81)	40 (11–162)	0.13	21 (11–53)	36 (21–66)	31 (12–202)	0.10
Fasting plasma glucose (mg/dl)	133 (96–207)	143 (87–414)	111 (76–167)	0.20	103 (93–220)	121 (83–198)	116 (88–199)	0.51
A1C (%)	8.2 (4.7–11.6)	8.0 (4.9–13.6)	6.2 (5.1–9.5)	0.27	6.0 (5.0–9.0)	6.2 (5.0–10.0)	7.0 (6.0–11.0)	0.10
HOMA-IR	3.9 (0.7–5.5)	3.4 (1.9–7.7)	3.9 (1.6–11.1)	0.91	3.1 (1.5–8.5)	3.4 (1.9–7.7)	3.9 (1.6–11.1)	0.76
QUICKI	0.32 (0.29–0.40)	0.31 (0.27–0.34)	0.31 (0.29–0.35)	0.32	0.33 (0.28–0.37)	0.32 (0.30–0.35)	0.31 (0.29–0.34)	0.82
Muscle insulin resistance	2.1 (1.5–4.0)	1.7 (0.3–3.3)	3.0 (2.1–4.4)	0.20	2.0 (1.3–5.9)	2.4 (1.6–4.5)	1.9 (1.3–4.5)	0.80
Hepatic insulin resistance (×10^6)	5.3 (2.3–10.2)	5.0 (2.3–10.0)	3.7 (1.4–10.6)	0.66	3.9 (1.4–9.8)	4.3 (1.9–15.9)	4.5 (2.3–8.8)	0.75
Total cholesterol (mg/dl)	191 (128–276)	187 (129–252)	206 (163–244)	0.57	192 (114–224)	195 (136–273)	194 (162–234)	0.74
Triglycerides (mg/dl)	111 (28–224)	114 (36–204)	96 (36–521)	0.87	104 (22–241)	115 (57–241)	131 (36–173)	0.68
HDL cholesterol (mg/dl)	47 (35–82)	51 (31–73)	48 (20–74)	0.68	53 (40–71)	52 (39–64)	52 (36–79)	0.92
Platelets (×10^4/μl)	21.1 (9.4–30.8)	23.0 (7.0–38.2)	24.3 (20.2–41.2)	0.29	23.3 (14.5–27.6)	21.5 (6.3–31.8)	24.0 (15.2–32.6)	0.60
Ferritin (μg/dl)	185 (13–452)	397 (190–604)	46 (10–347)	0.14	74 (16–211)	162 (110–614)	62 (10–171)	0.05
hs-CRP	0.40 (0.08–7.53)	0.14 (0.02–0.61)	0.06 (0.00–0.30)	0.23	0.09 (0.04–0.23)	0.10 (0.00–0.24)	0.09 (0.00–0.89)	0.89
Type IV collagen 7S (ng/dl)	5.1 (2.7–10.0)	4.1 (3.1–7.2)	3.7 (3.3–4.5)	0.27	3.5 (2.3–3.9)	8.3 (3.2–14.0)	4.0 (3.2–5.0)	0.21
HA (ng/dl)	20.6 (0.0–144.7)	25.5 (11.5–299)	30.4 (0.0–61.7)	0.66	32.8 (0.0–117.2)	24.5 (0.0–570)	24.3 (0.0–140.3)	0.63
P-III-P (U/ml)	0.6 (0.5–1.2)	0.6 (0.4–45.0)	0.5 (0.4–0.6)	0.07	0.6 (0.3–0.8)	0.5 (0.5–233.0)	0.6 (0.4–1.0)	0.96
Diabetes (%)	82	69	64	0.59	82	75	64	0.56
Dyslipidemia (%)	73	63	73	0.95	73	63	73	0.86
Hypertension (%)	64	18	36	0.03	64	18	36	0.10
Metabolic syndrome (%)	73	38	27	0.18	67	50	45	0.43
ΔA1C					−1.9 (−6.0 to 0.4)	−1.2 (−6.1 to 4.4)	0.3 (−1.8 to 7.1)	0.02
ΔBody weight					−4.7 (−10.6 to 10.2)	2.2 (−9.4 to 13.4)	−0.9 (−12.7 to 9.6)	0.04
ΔHOMA-IR					−1.3 (−4.4 to 1.2)	−0.3 (−4.3 to 3.3)	−0.7 (−6.1 to 1.8)	0.81

Data are medians (range) or %. A Kruskal-Wallis test and a χ^2 test were used to compare the continuous and categorical variables among three groups. HA, hyaluronic acid; hs-CRP, high-sensitivity C-reactive protein; P-III-P, procollagen III peptide.

Liver fibrosis improved in 12 patients (30.7%), progressed in 11 patients (28.2%), and remained unchanged in 16 patients (41%). As shown in Table 1, fasting plasma glucose, A1C, insulin resistance indicators, and prevalence of metabolic disorders were not significantly different among the three liver fibrosis groups. In the Cox proportional hazard model (supplementary Table 3), although some of the confidence intervals were very wide because of the small sample size, improvement of liver fibrosis was significantly associated with changes in A1C between the initial and final liver biopsies (ΔA1C) ($P = 0.005$) and use of insulin for the treatment of diabetes ($P = 0.019$). Both ΔA1C and use of insulin were independently associated with the improvement of liver fibrosis after adjusted for each other. However, ΔA1C was more strongly associated with the improvement of liver fibrosis than use of insulin (χ^2; 7.97 vs. 4.58, respectively; supplementary Table 3).

CONCLUSIONS — In the present study, we showed that a change in glycemic control (ΔA1C), but not changes in insulin resistance indicators, was an independent predictor of the progression of liver fibrosis in Japanese patients with NAFLD. This is the first report identifying a change in A1C as a predictor of the histological course in the liver of patients with NAFLD. Two of five previous longitudinal studies have identified obesity, higher BMI, and homeostasis model assessment of insulin resistance (HOMA-IR) as predictors of liver fibrosis progression in Western populations (4,5). The difference between those results and the results of the present study may be due in part to differences in the assessed severity of obesity and insulin resistance between the populations. We previously demonstrated that diabetes is an independent risk factor for the progression of liver fibrosis in hepatitis C (6) and that diabetes accelerates the pathology of nonalcoholic steatohepatitis in the type 2 diabetic rat model OLETF (7).

Liver fibrosis is closely associated with two regulators of fibrosis: transforming growth factor (TGF)-β (8,9) and plasminogen activator inhibitor type 1 (PAI-1) (8,10). High glucose levels induce the expression of TGF-β (11) and PAI-1 (12). We previously reported that the expression of TGF family member genes, PAI-1, and genes involved in fibrogenesis are upregulated in the livers of patients with type 2 diabetes (13,14), suggesting that a diabetic state increases the risk for liver fibrosis.

In the present study, only ΔA1C was associated with the progression of liver fibrosis, but not liver inflammation (data not shown). We speculate that the reduction of A1C inhibits the expression of master genes such as *TGF-β* and *PAI-1* that are involved in the regulation of fibrogenesis, rather than genes involved in liver inflammation, and thereby improves liver fibrosis in NAFLD.

The major limitation of this study was small population size. We could not evaluate the changes of liver histology according to the difference in detail characteristics such as treatment of diabetes. Lower statistical power of this study should be consider when we evaluate the results.

In conclusion, our study suggested that ΔA1C could predict liver fibrosis progression in Japanese patients with NAFLD, and tight glycemic control may ameliorate liver fibrosis. Future large-scale prospective studies are needed to confirm our results.

Acknowledgments— This study was supported in part by a grant-in-aid from the Ministry of Education, Culture, Sports, Science and Technology, Japan.

No potential conflicts of interest relevant to this article were reported.

We thank Dr. Akiko Shimizu, Dr. Tsuguhito Ota, and Dr. Hirofumi Misu for recruiting the patients.

References

1. Duvnjak M, Lerotic I, Barsic N, Tomasic V, Virovic Jukic L, Velagic V. Pathogenesis and management issues for non-alcoholic fatty liver disease. World J Gastroenterol 2007;13:4539–4550
2. Sakurai M, Takamura T, Ota T, Ando H, Akahori H, Kaji K, Sasaki M, Nakanuma Y, Miura K, Kaneko S. Liver steatosis, but not fibrosis, is associated with insulin resistance in nonalcoholic fatty liver disease. J Gastroenterol 2007;42:312–317
3. Brunt EM, Janney CG, Di Bisceglie AM, Neuschwander-Tetri BA, Bacon BR. Nonalcoholic steatohepatitis: a proposal for grading and staging the histological lesions. Am J Gastroenterol 1999;94:2467–2474
4. Ekstedt M, Franzen LE, Mathiesen UL, Thorelius L, Holmqvist M, Bodemar G, Kechagias S. Long-term follow-up of patients with NAFLD and elevated liver enzymes. Hepatology 2006;44:865–873
5. Fassio E, Alvarez E, Dominguez N, Landeira G, Longo C. Natural history of nonalcoholic steatohepatitis: a longitudinal study of repeat liver biopsies. Hepatology 2004;40:820–826
6. Kita Y, Mizukoshi E, Takamura T, Sakurai M, Takata Y, Arai K, Yamashita T, Nakamoto Y, Kaneko S. Impact of diabetes mellitus on prognosis of patients infected with hepatitis C virus. Metabolism 2007;56:1682–1688
7. Ota T, Takamura T, Kurita S, Matsuzawa N, Kita Y, Uno M, Akahori H, Misu H, Sakurai M, Zen Y, Nakanuma Y, Kaneko S. Insulin resistance accelerates a dietary rat model of nonalcoholic steatohepatitis. Gastroenterology 2007;132:282–293
8. Matsuzawa N, Takamura T, Kurita S, Misu H, Ota T, Ando H, Yokoyama M, Honda M, Zen Y, Nakanuma Y, Miyamoto K, Kaneko S. Lipid-induced oxidative stress causes steatohepatitis in mice fed an atherogenic diet. Hepatology 2007;46:1392–1403
9. Uno M, Kurita S, Misu H, Ando H, Ota T, Matsuzawa-Nagata N, Kita Y, Nabemoto S, Akahori H, Zen Y, Nakanuma Y, Kaneko S, Takamura T. Tranilast, an antifibrogenic agent, ameliorates a dietary rat model of nonalcoholic steatohepatitis. Hepatology 2008;48:109–118
10. Bergheim I, Guo L, Davis MA, Lambert JC, Beier JI, Duveau I, Luyendyk JP, Roth RA, Arteel GE. Metformin prevents alcohol-induced liver injury in the mouse: critical role of plasminogen activator inhibitor-1. Gastroenterology 2006;130:2099–2112
11. Sugimoto R, Enjoji M, Kohjima M, Tsuruta S, Fukushima M, Iwao M, Sonta T, Kotoh K, Inoguchi T, Nakamuta M. High glucose stimulates hepatic stellate cells to proliferate and to produce collagen through free radical production and activation of mitogen-activated protein kinase. Liver Int 2005;25:1018–1026
12. Suzuki M, Akimoto K, Hattori Y. Glucose upregulates plasminogen activator inhibitor-1 gene expression in vascular smooth muscle cells. Life Sci 2002;72:59–66
13. Takamura T, Sakurai M, Ota T, Ando H, Honda M, Kaneko S. Genes for systemic vascular complications are differentially expressed in the livers of type 2 diabetic patients. Diabetologia 2004;47:638–647
14. Takeshita Y, Takamura T, Hamaguchi E, Shimizu A, Ota T, Sakurai M, Kaneko S. Tumor necrosis factor-alpha-induced production of plasminogen activator inhibitor 1 and its regulation by pioglitazone and cerivastatin in a nonmalignant human hepatocyte cell line. Metabolism 2006;55:1464–1472

GASTROENTEROLOGY 2009;136:1012–1024

EpCAM-Positive Hepatocellular Carcinoma Cells Are Tumor-Initiating Cells With Stem/Progenitor Cell Features

TARO YAMASHITA,* JUNFANG JI,* ANURADHA BUDHU,* MARSHONNA FORGUES,* WEN YANG,‡ HONG-YANG WANG,‡ HULIANG JIA,§ QINGHAI YE,§ LUN-XIU QIN,§ ELAINE WAUTHIER,‖ LOLA M. REID,‖ HIROSHI MINATO,¶ MASAO HONDA,¶ SHUICHI KANEKO,¶ ZHAO-YOU TANG,§ and XIN WEI WANG*

*Liver Carcinogenesis Section, Laboratory of Human Carcinogenesis, Center for Cancer Research, National Cancer Institute, Bethesda, Maryland; ‡International Cooperation Laboratory on Signal Transduction, Eastern Hepatobiliary Surgery Institute, Shanghai, China; §Liver Cancer Institute and Zhongshan Hospital, Fudan University, Shanghai, China; ‖Department of Cell and Molecular Physiology, University of North Carolina School of Medicine, Chapel Hill, North Carolina; and the ¶Liver Disease Center and Kanazawa University Hospital, Kanazawa University, Kanazawa, Japan

Background & Aims: **Cancer progression/metastases and embryonic development share many properties including cellular plasticity, dynamic cell motility, and integral interaction with the microenvironment. We hypothesized that the heterogeneous nature of hepatocellular carcinoma (HCC), in part, may be owing to the presence of hepatic cancer cells with stem/progenitor features.** ***Methods:*** **Gene expression profiling and immunohistochemistry analyses were used to analyze 235 tumor specimens derived from 2 recently identified HCC subtypes (EpCAM$^+$ α-fetoprotein [AFP$^+$] HCC and EpCAM$^-$ AFP$^-$ HCC). These subtypes differed in their expression of AFP, a molecule produced in the developing embryo, and EpCAM, a cell surface hepatic stem cell marker. Fluorescence-activated cell sorting was used to isolate EpCAM$^+$ HCC cells, which were tested for hepatic stem/progenitor cell properties.** ***Results:*** **Gene expression and pathway analyses revealed that the EpCAM$^+$ AFP$^+$ HCC subtype had features of hepatic stem/progenitor cells. Indeed, the fluorescence-activated cell sorting–isolated EpCAM$^+$ HCC cells displayed hepatic cancer stem cell–like traits including the abilities to self-renew and differentiate. Moreover, these cells were capable of initiating highly invasive HCC in nonobese diabetic, severe combined immunodeficient mice. Activation of Wnt/β-catenin signaling enriched the EpCAM$^+$ cell population, whereas RNA interference-based blockage of EpCAM, a Wnt/β-catenin signaling target, attenuated the activities of these cells.** ***Conclusions:*** **Taken together, our results suggest that HCC growth and invasiveness is dictated by a subset of EpCAM$^+$ cells, opening a new avenue for HCC cancer cell eradication by targeting Wnt/β-catenin signaling components such as EpCAM.**

Tumors originate from normal cells as a result of accumulated genetic/epigenetic changes. Although considered monoclonal in origin, tumor cells are heterogeneous in their morphology, clinical behavior, and molecular profiles.[1,2] Tumor cell heterogeneity has been explained previously by the clonal evolution model[3]; however, recent evidence has suggested that heterogeneity may be owing to derivation from endogenous stem/progenitor cells[4] or de-differentiation of a transformed cell.[5] This hypothesis supports an early proposal that cancers represent "blocked ontogeny"[6] and a derivative that cancers are transformed stem cells.[7] This renaissance of stem cells as targets of malignant transformation has led to realizations about the similarities between cancer cells and normal stem cells in their capacity to self-renew, produce heterogeneous progenies, and limitlessly divide.[8] The cancer stem cell (CSC) (or tumor-initiating cell) concept is that a subset of cancer cells bear stem cell features that are indispensable for a tumor. Accumulating evidence suggests the involvement of CSCs in the perpetuation of various cancers including leukemia, breast cancer, brain cancer, prostate cancer, and colon cancer.[9–13] Experimentally, putative CSCs have been isolated using cell surface markers specific for normal stem cells. Stem cell–like features of CSC have been confirmed by functional in vitro clonogenicity and in vivo tumorigenicity assays. For example, leukemia-initiating cells in nonobese diabetic, severe combined immunodeficient (NOD/SCID) mice are CD34^{++}CD38$^-$.[11] Breast cancer CSCs are CD44$^+$CD24$^{-/low}$ cells, whereas tumor-initiating cells of the brain, colon, and prostate are CD133$^+$.[10,12,13] CSCs are considered more metastatic and drug-/radiation-resistant than non-CSCs in the tumor, and are responsible for cancer relapse. These findings warrant the development of treatment strategies that can specifically eradicate CSCs.[14,15]

Abbreviations used in this paper: AFP, α-fetoprotein; BIO, 6-bromoindirubin-3′-oxime; CSC, cancer stem cell; FACS, fluorescence-activated cell sorting; 5-FU, 5-fluorouracil; HpSC, hepatic stem cell; IF, immunofluorescence; IHC, immunohistochemistry; MACS, magnetic-activated cell sorting; MeBIO, 1-methyl-BIO; MH, mature hepatocyte; PCNA, proliferating cell nuclear antigen; siRNA, small interfering RNA.

0016-5085/09/$36.00
doi:10.1053/j.gastro.2008.12.004

Hepatocellular carcinoma (HCC) is the third leading cause of cancer death worldwide.[16] Although the cellular origin of HCC is unclear,[17,18] HCC has heterogeneous pathologies and genetic/genomic profiles,[19] suggesting that HCC can initiate in different cell lineages.[20] The liver is considered as a maturational lineage system similar to that in the bone marrow.[21] Experimental evidence indicates that certain forms of hepatic stem cells (HpSCs), present in human livers of all donor ages, are multipotent and can give rise to hepatoblasts,[22,23] which are, in turn, bipotent progenitor cells that can progress either into hepatocytic or biliary lineages.[22,24] α-fetoprotein (AFP) is one of the earliest markers detected in the liver bud specified from the ventral foregut,[25,26] but its expression has been found only in hepatoblasts and to a lesser extent in committed hepatocytic progenitors, not in later lineages or in normal human HpSC.[22] Recent studies also have indicated that EpCAM is a biomarker for HpSC because it is expressed in HpSCs and hepatoblasts.[22-24]

We recently identified a novel HCC classification system based on EpCAM and AFP status.[27] Gene expression profiles revealed that EpCAM$^+$ AFP$^+$ HCC (referred to as *HpSC-HCC*) has progenitor features with poor prognosis, whereas EpCAM$^-$ AFP$^-$ HCC (referred to as *mature hepatocyte-like HCC*; MH-HCC) have adult hepatocyte features with good prognosis. Wnt/β-catenin signaling, a critical player for maintaining embryonic stem cells,[28] is activated in EpCAM$^+$ AFP$^+$ HCC, and EpCAM is a direct transcriptional target of Wnt/β-catenin signaling.[29] Moreover, EpCAM$^+$ AFP$^+$ HCC cells are more sensitive to β-catenin inhibitors than EpCAM$^-$ HCC cells in vitro.[29] Interestingly, a heterogeneous expression of EpCAM and AFP was observed in clinical tissues, a feature that may be attributed to the presence of a subset of CSCs. In this study, we have confirmed that EpCAM$^+$ HCC cells are highly invasive and tumorigenic, and have activated Wnt/β-catenin signaling. We also show a crucial role of EpCAM in the maintenance of hepatic CSCs. Our data shed new light on the pathogenesis of HCC and may open new avenues for therapeutic interventions for targeting hepatic CSCs.

Materials and Methods

Clinical Specimens

HCC samples were obtained with informed consent from patients who underwent radical resection at the Liver Cancer Institute of Fudan University, Eastern Hepatobiliary Surgery Institute, and the Liver Disease Center of Kanazawa University Hospital, and the study was approved by the institutional review boards of the respective institutes. The microarray data from clinical specimens are available publicly (GEO accession number, GSE5975).[27] Array data from a total of 156 HCC cases (155 hepatitis B virus [HBV]-positive) corresponding to 2 subtypes of HCC (ie, HpSC-HCC and MH-HCC), were used to search for HpSC-HCC–associated genes (Supplementary Table 1; see supplementary material online at www.gastrojournal.org). A total of 79 formalin-fixed and paraffin-embedded HCC samples were used for immunohistochemistry (IHC) analyses (Supplementary Table 2; see supplementary material online at www.gastrojournal.org), 56 of which also were used in a recent study.[30] The classification of HpSC-HCC and MH-HCC was based on previously described criteria.[27]

Cell Cultures and Sorting

Human liver cancer cell lines (HuH1 and HuH7) were derived from Health Science Research Resources Bank (JCRB0199 and JCRB0403, respectively) and routinely cultured as previously described.[31] Normal human MHs, provided by the University of Pittsburgh through Liver Tissue Cell Distribution System, were cultured as previously described.[32] Human HpSCs were isolated from fetal livers and cultured in Kubota and Reid's[33] medium as previously described. Wnt10B conditioned medium was prepared as described.[34] Embryonic stem cell culture medium was prepared using Knockout Dulbecco's modified Eagle medium supplemented with 18% of Serum Replacement (Invitrogen, Carlsbad, CA). The pTOP-FLASH and pFOP-FLASH luciferase constructs were described previously.[29] BIO and MeBIO were generous gifts from Ali Brivanlou (The Rockefeller University, New York, NY). For isolating single cell–derived colonies to determine whether heterogeneity is an intrinsic property of EpCAM$^+$ cells, HuH1 and HuH7 cells were resuspended and plated as a single cell per well in 96-well plates. A total of 192 single cells were plated successfully. The clones that grew well were selected 2 weeks after seeding and used for immunofluorescence (IF) analysis. The 5-fluorouracil (5-FU) stock (2 mg/mL; Sigma, St Louis, MO), was prepared in distilled water. Fluorescence-activated cell sorting (FACS) and magnetic-activated cell sorting (MACS) analyses were used to isolate EpCAM$^+$ HCC cells (Supplementary materials; see supplementary Materials and Methods online at www.gastrojournal.org).

Clonogenicity, Spheroid Formation, Invasion, Quantitative Reverse Transcription–Polymerase Chain Reaction, and IHC Assays

For colony formation assays, 2000 EpCAM$^+$ or EpCAM$^-$ cells were seeded in 6-well plates after FACS. After 10 days of culture, cells were fixed by 100% methanol and stained with methylene blue. For spheroid assays, single-cell suspensions of 1000 EpCAM$^+$ or EpCAM$^-$ cells were seeded in 6-well Ultra-Low Attachment Microplates (Corning, Corning, NY) after FACS. The number of spheroids was measured 14 days after seeding. Invasion assays were performed using BD BioCoat Matrigel Matrix Cell Culture Inserts and Control Inserts (BD Biosciences, San Jose, CA) essentially as pre-

viously described.[31] Reverse transcription-polymerase chain reaction and IHC assays are described in detail in the supplementary materials (see supplementary material online at www.gastrojournal.org).

Tumorigenicity in NOD/SCID Mice

Six-week-old NOD/SCID mice (NOD/NCrCRl-*Prkdc*^{scid}) were purchased from Charles River (Charles River Laboratories, Inc, Wilmington, MA). The protocol was approved by the National Cancer Institute-Bethesda Animal Care and Use Committee. Cells were suspended in 200 μL of Dulbecco's modified Eagle medium and Matrigel (1:1), and a subcutaneous injection was performed. The size and incidence of subcutaneous tumors were recorded. For histologic evaluation, tumors were formalin-fixed, paraffin-embedded or embedded directly in OCT compound (Sakura Finetek, Torrance, CA) and stored at −80°C.

RNA Interference

A small interfering RNA (siRNA) specific to *TACSTD1* (SI03019667) and a control siRNA (1022076) were designed and synthesized by Qiagen (Qiagen, Valencia, CA). Transfection was performed using Lipofectamine 2000 (Invitrogen), according to the manufacturer's instructions. A total of 200 nmol/L of siRNA duplex was used for each transfection.

Statistical Analyses

The class comparison and gene clustering analyses were performed as previously described.[30] The canonic pathway analysis was performed using Ingenuity Pathways Analysis (v5.5; Ingenuity Systems, Redwood City, CA). The association of HCC subtypes and clinicopathologic characteristics was examined using either the Mann-Whitney *U* test or the chi-square test. Student *t* tests were used to compare various test groups assayed by colony formation, spheroid formation, or invasion assays. The Kaplan-Meier survival analysis was performed to compare patient survival or tumorigenicity.

Results

A Poor Prognostic HCC Subtype With Molecular Features of HpSC

We re-evaluated the gene expression profiles that were uniquely associated with 2 recently identified prognostic subtypes of HCC (ie, HpSC-HCC and MH-HCC), using a publicly available microarray dataset of 156 HCC cases (GEO accession number: GSE5975). Sixty cases were defined as HpSC-HCC with a poor prognosis and 96 cases were defined as MH-HCC with a good prognosis, based on EpCAM and AFP status.[27] A class-comparison analysis with univariate *t* tests and a global permutation test (1000×) yielded 793 genes that were expressed differentially between HpSC-HCC and MH-HCC ($P < .001$). Hierarchical cluster analyses revealed 2 main gene clusters that were up-regulated (cluster A; 455 genes) or down-regulated (cluster B; 338 genes) in HpSC-HCC (Figure 1*A*). Pathway analysis indicated that the enriched genes in cluster A were associated significantly with known stem cell signaling pathways such as transforming growth factor-β, Wnt/β-catenin, PI3K/Akt, and integrin ($P < .01$) (Figure 1*B*). In contrast, genes in cluster B were associated significantly with mature hepatocyte functions such as xenobiotic metabolism, complement system, and coagulation system ($P < .01$). Noticeably, known HpSC markers such as *KRT19* (CK19), *TACSTD1* (EpCAM), *AFP*, *DKK1*, *DLK1*, and *PROM1* (CD133) were up-regulated significantly in HpSC-HCC, whereas known liver maturation markers such as *UGT2B7* and *CYP3A4* were expressed more abundantly in MH-HCC (Figure 1*C* and Supplementary Tables 3 and 4; see supplementary material online at www.gastrojournal.org). Kaplan-Meier survival analysis revealed that HpSC-HCC patients had a significantly shorter survival than MH-HCC patients ($P = .036$) (Figure 1*D*). Consistently, HpSC-HCC patients had a high frequency of macroscopic and microscopic portal vein invasion (Figure 1*E*).

However, IHC analyses of an additional 79 HCC cases revealed that among 24 HpSC-HCC cases, EpCAM staining was very heterogeneous with a mixture of EpCAM$^+$ and EpCAM$^-$ tumor cells in each tumor (Figure 1*F*, *left panel*). Noticeably, many of the EpCAM$^+$ tumor cells were located at the invasion border zones and often were disseminated at the invasive front (*black arrows*). IF analysis revealed that HCC cells located at the invasive front co-expressed EpCAM, CK19, and AFP (Figure 1*F*, *right panels*). Noticeably, HpSC-HCC patients were significantly younger than MH-HCC patients (Supplementary Tables 1 and 2; see supplementary material online at www.gastrojournal.org). Enrichment of EpCAM$^+$ AFP$^+$ tumor cells at the tumor-invasive front suggested their involvement in HCC invasion and metastasis.

Isolation and Characterization of EpCAM$^+$ Cells in HCC

The results described earlier suggest that HpSC-HCC may be organized in a hierarchical fashion in which EpCAM$^+$ tumor cells act as stem-like cells with an ability to differentiate into EpCAM$^-$ tumor cells. To test this hypothesis, we first evaluated the expression pattern of 7 hepatic stem/maturation markers (EpCAM, CD133, CD90, CK19, Vimentin, Hep-Par1, and β-catenin) in 6 HCC cell lines (Figure 2*A*). All 3 AFP$^+$ cell lines (HuH1, HuH7, and Hep3B) expressed EpCAM, CD133, and cytoplasmic/nuclear β-catenin, whereas the other 3 AFP$^-$ cell lines (SK-Hep-1, HLE, and HLF) did not, consistent with the microarray data. Interestingly, AFP$^+$ cell lines had no CD90$^+$ cell population, which recently was identified as hepatic CSCs,[35] whereas AFP$^-$ cell lines had such a population. Consistent with the IF data, FACS analysis showed that AFP$^+$ cell lines had a subpopulation of

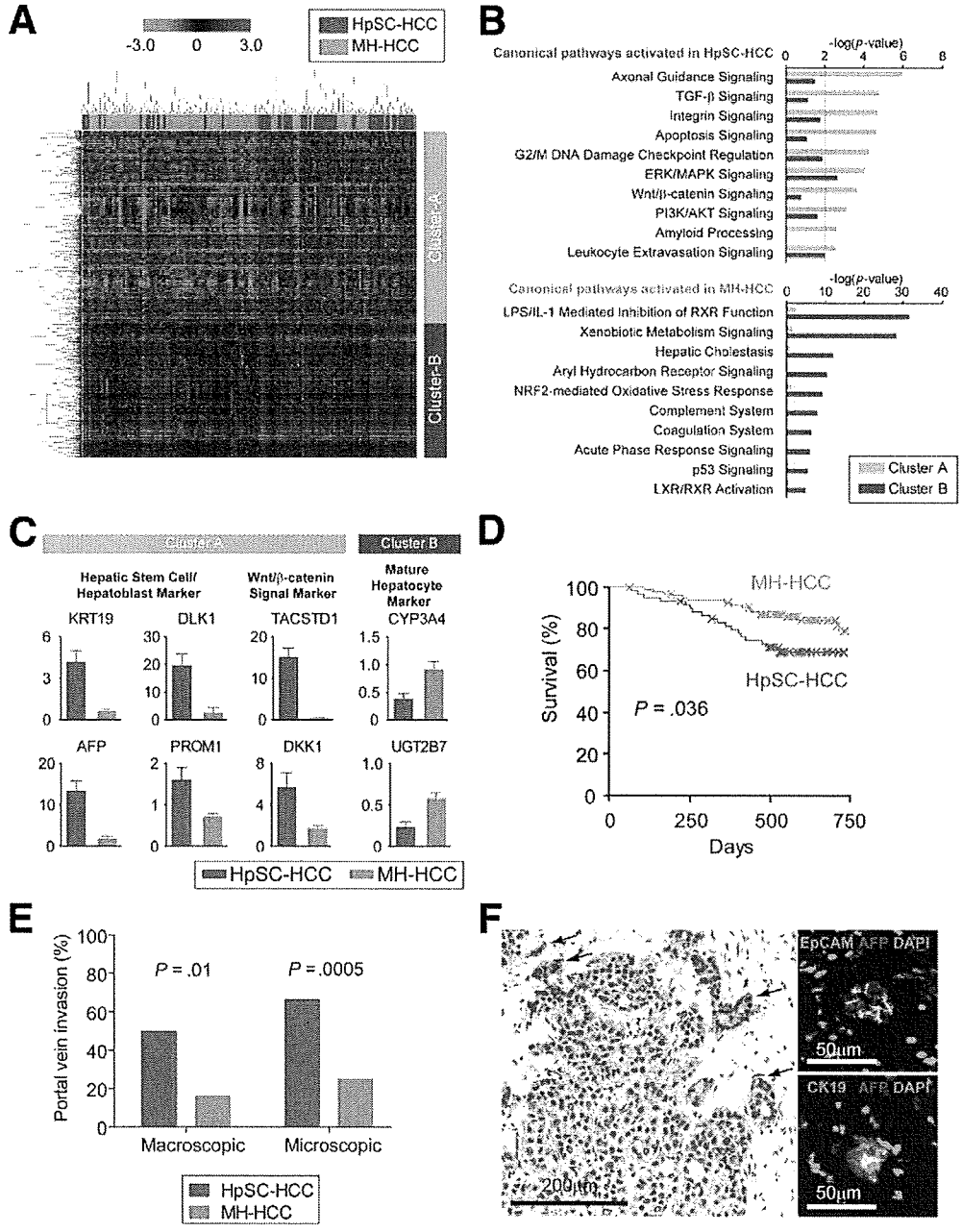

Figure 1. HpSC–HCC represents a subset of invasive HCCs with CSC features. (*A*) Hierarchical cluster analysis based on 793 HpSC–HCC–coregulated genes in 156 HCC cases. Each cell in the matrix represents the expression level of a gene in an individual sample. Red and green cells depict high and low expression levels, respectively, as indicated by the scale bar. (*B*) Pathway analysis of HpSC–HCC–coregulated genes. The top 10 canonical signaling pathways activated in cluster A (*upper panel*) or cluster B (*lower panel*) with statistical significance ($P < .01$) are shown. (*C*) Expression patterns of well-known HpSC and MH markers in each HCC subtype as analyzed by microarray. (*D*) Kaplan–Meier survival analysis of the cases used for array analysis. (*E*) Frequency of macroscopic and microscopic portal vein invasion in HpSC-HCC and MH-HCC used for IHC. (*F*) Representative images of EpCAM, AFP, and CK19 staining in HpSC–HCC samples analyzed by IHC and IF. EpCAM staining illustrates heterogeneous expression of EpCAM in HpSC-HCC (*left panel*). EpCAM$^+$ cells were disseminated in the invasive border (*left panel black arrows*) with expression of AFP (*right top panel*) and CK19 (*right bottom panel*).

EpCAM$^+$ and CD133$^+$, but no CD90$^+$ cells, whereas AFP$^-$ cell lines had a subpopulation of CD90$^+$ cells but no EpCAM$^+$ or CD133$^+$ cells (Figure 2*B*). These data indicate that HpSC-HCC and MH-HCC cell lines have distinct stem cell marker expression patterns, and EpCAM as well as CD133 may be hepatic CSC markers specifically in HpSC-HCC.

We selected 2 human HCC cell lines (HuH1 and HuH7) to isolate EpCAM$^+$ cells because both lines were heterogeneous in EpCAM, AFP, CK19, and β-catenin expression (Figure 2*A* and *B* and Supplementary Figure 1*A*; see supplementary material online at www.gastrojournal.org).[29] We successfully enriched EpCAM$^+$ and EpCAM$^-$ populations from HuH7 cells by FACS, with more than 80% purity in EpCAM$^+$ cells and more than 90% purity in EpCAM$^-$ cells 1 day after sorting (Figure 3*A*). Similar results were obtained when the purity check was performed immediately after sorting (data not shown). EpCAM$^+$ cells also were positive for CK19 and β-catenin (Figure 3*B* and Supplementary Figure 1*B*; see supplementary material online at www.gastrojournal.org) and most were AFP$^+$ (data not shown). In contrast, EpCAM$^-$ cells were negative for these markers but positive for HepPar1, a monoclonal antibody specific to hepatocytes (Figure 3*B*). Consistent with the microarray data described earlier, the levels of *TACSTD1*, *MYC*, and *hTERT* (known HpSC markers) were increased significantly in EpCAM$^+$ HuH7 cells, whereas the levels of *UGT2B7* and *CYP3A4*

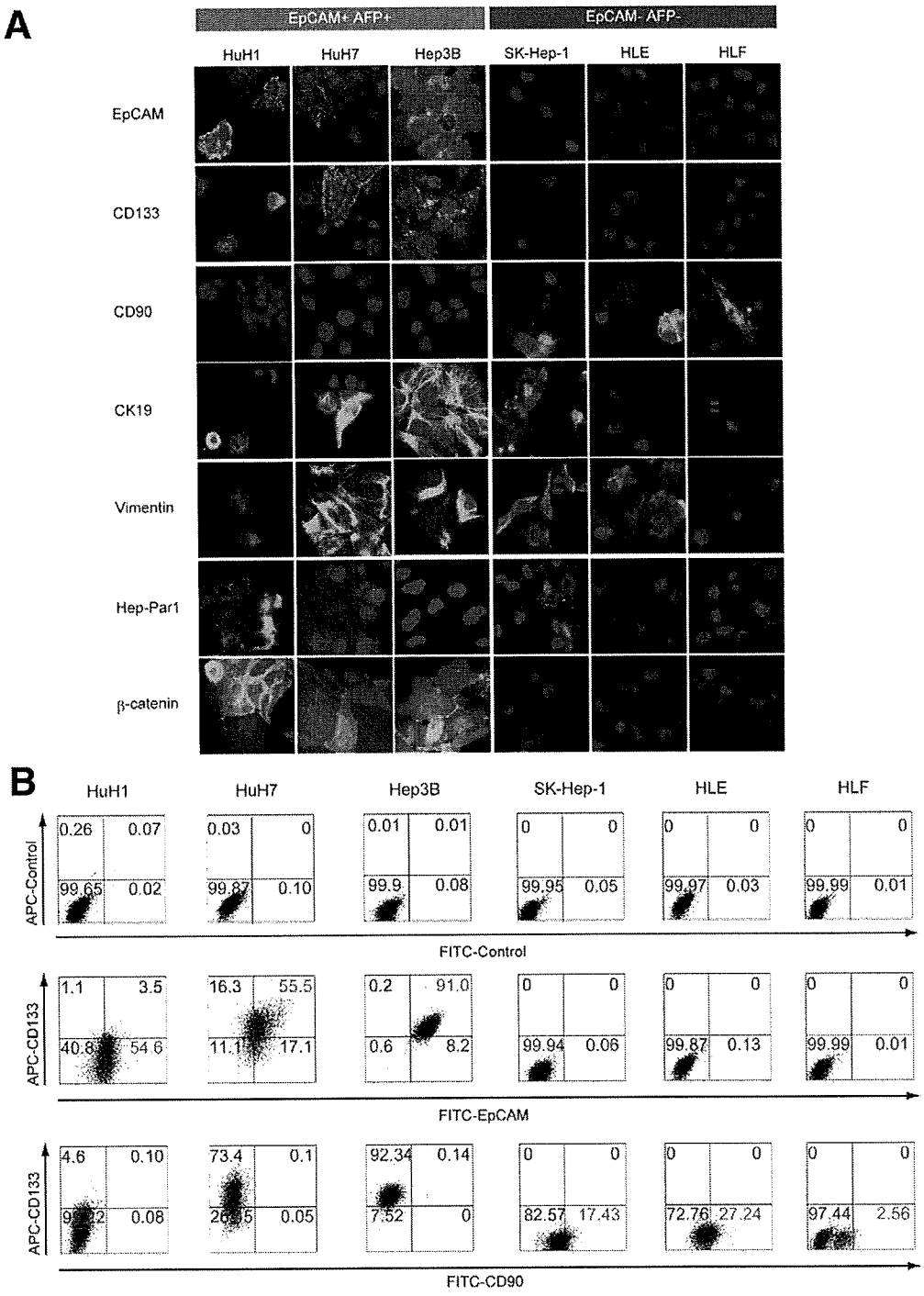

Figure 2. Characterization of hepatic stem cell marker expression in HCC cell lines. (*A*) IF analysis of 6 HCC cell lines (EpCAM$^+$ AFP$^+$ cell lines: HuH1, HuH7, and Hep3B; EpCAM$^-$ AFP$^-$ cell lines: SK-Hep-1, HLE, and HLF) stained with anti-EpCAM, anti-CD133, anti-CD90, anti-CK19, anti-Vimentin, anti–Hep-Par1, and anti–β-catenin antibodies. (*B*) FACS analysis of 6 HCC cell lines stained with anti-EpCAM, anti-CD133, and anti-CD90 antibodies.

(known mature hepatocyte markers) were significantly higher in EpCAM$^-$ HuH7 cells (Figure 3C, *left upper panel*). This expression pattern was reminiscent of human HpSC cells (Figure 3C, *left lower panel*). Similar results were obtained from HuH1 cells (data not shown). We also compared gene expression patterns of isolated HuH1, HuH7, MH, and HpSC cells using the TaqMan Human Stem Cell Pluripotency Array (Applied Biosystems, Foster City, CA) containing 96 selected human stem cell–related genes. Although a differential expression pattern of stem cell–related genes was evident among HpSC, EpCAM$^+$ HuH1, and EpCAM$^+$ HuH7 cells, the EpCAM$^+$ HCC cells were related more closely to HpSC cells whereas EpCAM$^-$ HCC cells were related more closely to diploid adult mature hepatocytes (Figure 3C, *right panel*; and Supplementary Figure 1C; see supplementary material online at www.gastrojournal.org). Thus, it appeared that EpCAM$^+$ HCC cells had a gene expression pattern that is related more closely to HpSC than EpCAM$^-$ HCC cells.

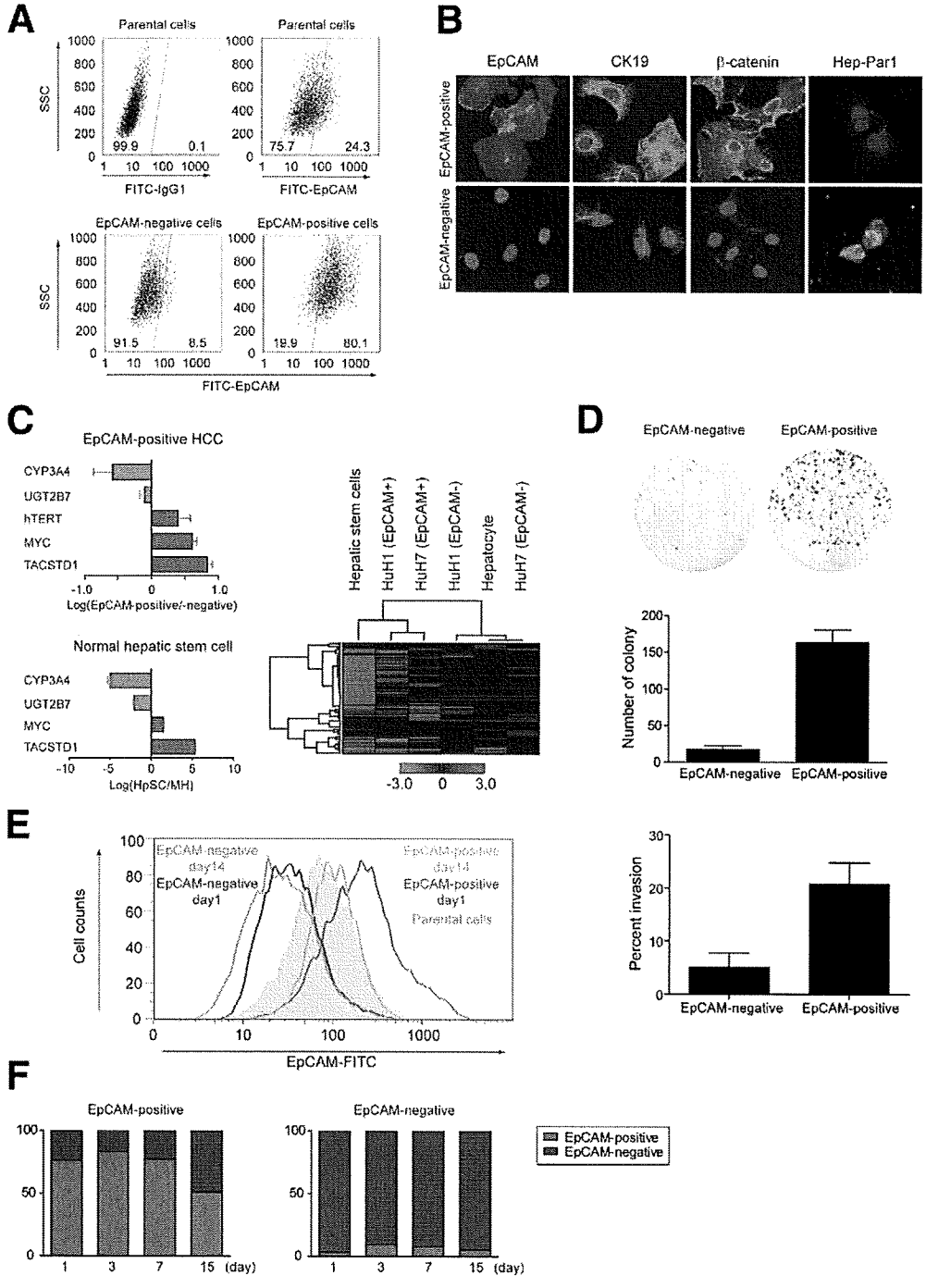

Figure 3. Characterization of EpCAM$^+$ and EpCAM$^-$ cells in HuH7 cells. (*A*) FACS analysis of EpCAM$^+$ and EpCAM$^-$ cells on day 1 after cell sorting. (*B*) IF analysis of cells stained with anti-EpCAM, anti-AFP, anti-CK19, or anti–β-catenin antibodies. (*C*) Quantitative reverse-transcription polymerase chain reaction analysis of EpCAM$^+$ and EpCAM$^-$ HuH7 cells (*left upper panel*) or HpSCs and MHs (*left lower panel*). Experiments were performed in triplicate. Hierarchical cluster analysis of HpSC, MH, and EpCAM$^+$ and EpCAM$^-$ HCC cells using a panel of genes expressed in human embryonic stem cells (*right panel*). Gene expression was measured in quadruplicate. (*D*) Representative photographs of the plates containing colonies derived from 2000 EpCAM$^+$ or EpCAM$^-$ HuH7 cells (*upper panel*). Colony formation experiments were performed in triplicate (mean ± SD) (*middle panel*). Cell invasiveness of EpCAM$^+$ and EpCAM$^-$ cells using the Matrigel invasion assay (*lower panel*). (*E*) Flow cytometer analysis of EpCAM$^+$ and EpCAM$^-$ HuH7 cells stained with anti-EpCAM at days 1 and 14 after cell sorting. (*F*) Percentage of sorted EpCAM$^+$ and EpCAM$^-$ cells after culturing for various times as analyzed by IF. Numbers of EpCAM$^+$ and EpCAM$^-$ cells were counted in 3 independent areas of chamber slides at days 1, 3, 7, and 15 after cell sorting. The average percentages of EpCAM$^+$ or EpCAM$^-$ cells are depicted as *red* or *blue*, respectively.

The isolated EpCAM$^+$ HuH7 cells formed colonies efficiently whereas EpCAM$^-$ cells failed to do so (Figure 3*D*, *upper* and *middle panels*; and Supplementary Figure 2*A* for HuH1 cells; see supplementary material online at www.gastrojournal.org). In addition, EpCAM$^+$ HuH7 cells were much more invasive than EpCAM$^-$ cells ($P <$ .03) (Figure 3*D*, *lower panel*; and Supplementary Figure 2*B* for HuH1 cells; see supplementary material online at www.gastrojournal.org). The EpCAM$^+$ fraction decreased with time in sorted EpCAM$^+$ HuH7 cells from greater than 80% to 50% (Figure 3*E*). However, a small percentage of EpCAM$^+$ cells remained constant in sorted EpCAM$^-$ HuH7 cells. FACS analysis confirmed the results of IF analysis (Figure 3*F* and Supplementary Figure 2*C* for HuH7 and HuH1 cells, respectively; see supplementary material online at www.gastrojournal.org), suggesting that EpCAM$^+$ cells could differentiate into EpCAM$^-$ cells, eventually allowing an enriched EpCAM$^+$ fraction to revert back to parental cells after 14 days of culture. In contrast, EpCAM$^-$ cells maintained their EpCAM$^-$ status. In addition, we successfully isolated 12 HuH1 and 2 HuH7 colonies from 192 single-cell–plated culture wells.

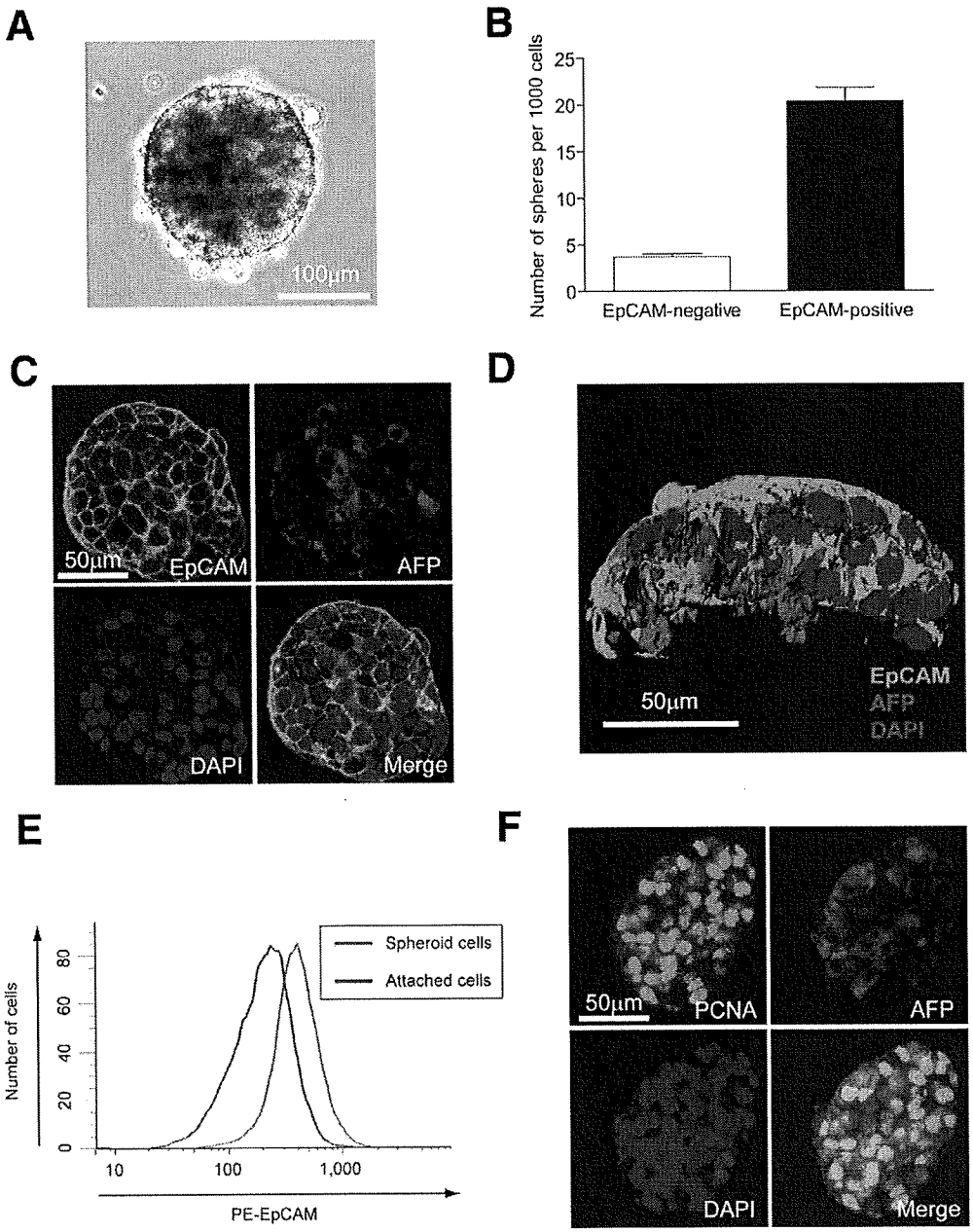

Figure 4. Spheroid formation of EpCAM$^+$ HuH1 HCC cells. (*A*) A representative phase-contrast image of an HCC spheroid derived from an EpCAM$^+$ cell (*scale bar*, 100 μm) and (*B*) total numbers of spheroids from 1000 sorted cells are shown. Experiments were performed in triplicate and data are shown as mean ± SD. (*C*) Representative confocal images of an HCC spheroid co-stained with anti-EpCAM, anti-AFP, and 4′,6-diamidino-2-phenylindole (DAPI) (*scale bar*, 50 μm). (*D*) A 3-dimensional image of an HCC spheroid co-stained with anti-EpCAM, anti-AFP, and DAPI (*scale bar*, 50 μm) reconstructed from confocal images using surface rendering. (*E*) FACS analysis of EpCAM$^+$ cells cultured as spheroid cells (*red*) or attached cells (*blue*) for 14 days after cell sorting. (*F*) Confocal images of an HCC spheroid co-stained with anti-PCNA, anti-AFP, and DAPI (*scale bar*, 50 μm).

However, all colonies were heterogeneous in EpCAM and AFP expression and no colony was completely EpCAM$^-$ (data not shown). Taken together, these results indicate that EpCAM$^+$ HCC cells resemble HpSC features. It appears that EpCAM$^+$ cells, but not EpCAM$^-$ cells, have self-renewal and differentiation capabilities with the ability to form colonies from a single cell, and produce both EpCAM$^+$ and EpCAM$^-$ cells.

It has been shown previously that stem/progenitor cells and cancer stem/progenitor cells can form spheroids in vitro in a nonattached condition.[36,37] Consistently, EpCAM$^+$ cells could form spheroids efficiently, reaching to about 150 to approximately 200 μm in diameter after 14 days of culture (Figure 4*A* and *B*). Interestingly, all cells in a spheroid were EpCAM$^+$, whereas AFP expression was relatively heterogeneous (Figure 4*C* and *D*, and Supplementary movie 1; see supplementary material online at www.gastrojournal.org). Rarely, a few spheroids derived from an EpCAM$^-$ cell fraction were positive for EpCAM (data not shown), suggesting that these spheroids were derived from contaminated residual EpCAM$^+$ cells by FACS sorting. All spheroid cells maintained EpCAM expression while half of the attached cells lost EpCAM expression when the EpCAM$^+$ fraction was cultured for 14 days (Figure 4*E*). Most spheroid cells also abundantly expressed proliferating cell nuclear antigen (PCNA), implying active cell proliferation (Figure 4*F* and Supplementary movie 2; see supplementary material online at www.gastrojournal.org). Thus, a subset of EpCAM$^+$ cells, but not EpCAM$^-$ cells, can form spheroids.

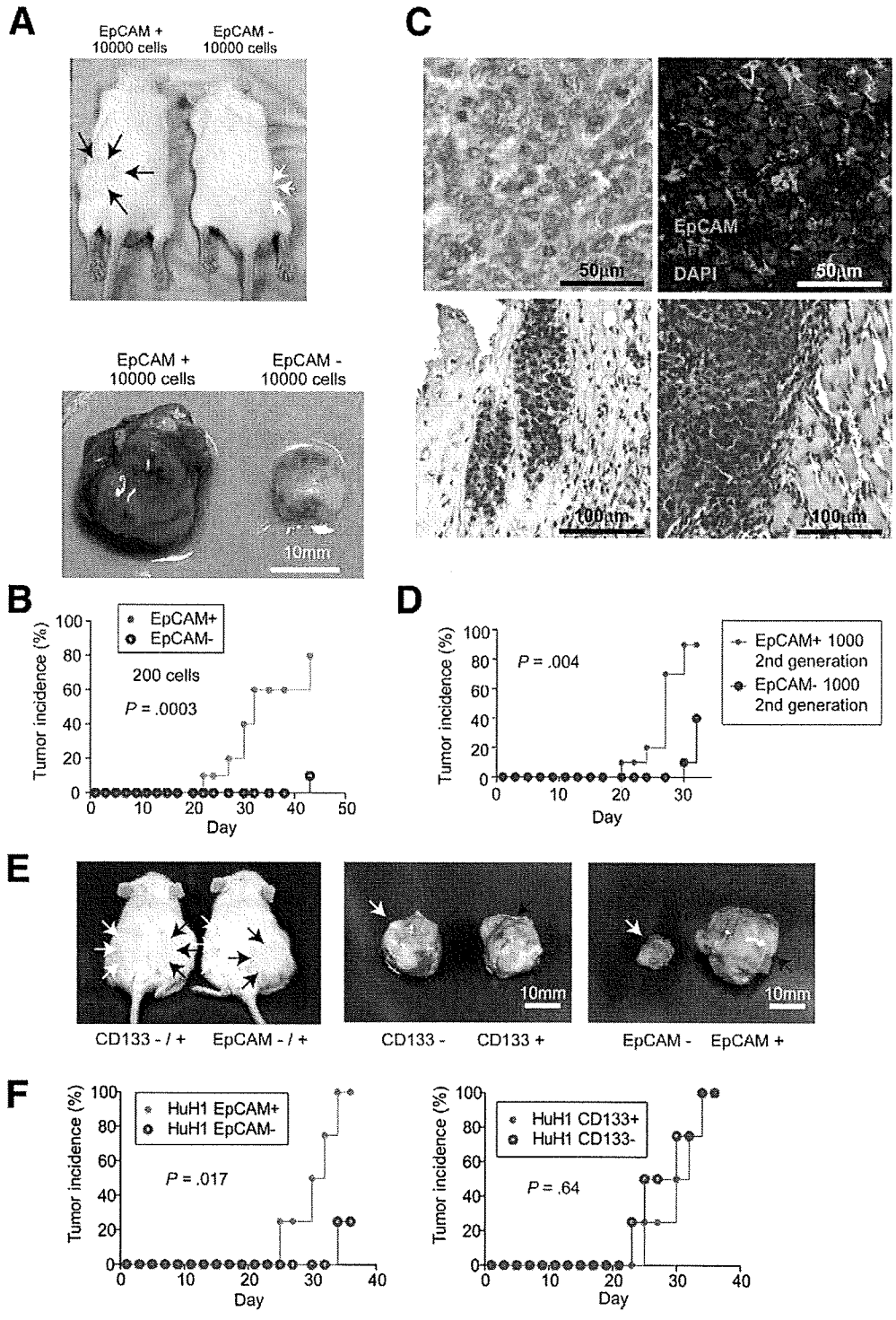

Figure 5. Tumorigenic and invasive potential of EpCAM$^+$ HCC cells. (*A*) Representative NOD/SCID mice (*upper panel*) with subcutaneous tumors (*lower panel*) from EpCAM$^+$ (*black arrows*) or EpCAM$^-$ (*white arrows*) HuH1 cells. (*B*) Tumorigenicity of 200 sorted HuH1 cells. (*C*) Histologic analysis of EpCAM$^+$ HuH1-derived xenografts. H&E staining of a subcutaneous tumor (*left upper panel*) with capsular invasion (*left lower panel*) and muscular invasion (*right lower panel*) and IF of the tumor stained with anti-EpCAM, anti-AFP, and 4′,6-diamidino-2-phenylindole (DAPI) (*right upper panel*) (*scale bar*, 50 μm). (*D*) Tumorigenicity of 1000 sorted cells derived from an EpCAM$^+$ HuH1 xenograft. Data are generated from 10 mice in each group. (*E*) Representative NOD/SCID mice (*left panel*) with subcutaneous tumors from CD133$^+$ (*black arrows*) or CD133$^-$ (*white arrows*) (*middle panel*) and EpCAM$^+$ (black arrows) or EpCAM$^-$ (*white arrows*) (*right panel*) HuH1 cells. (*F*) Tumorigenicity of 1000 HuH1 cells sorted by anti-EpCAM (*left panel*) or anti-CD133 (*right panel*) antibodies.

EpCAM$^+$ HCC Cells as Tumor-Initiating Cells

EpCAM$^+$ HCC cells, but not EpCAM$^-$ HCC cells, could efficiently initiate invasive tumors in NOD/SCID mice (Figure 5). For example, 10,000 EpCAM$^+$ HuH1 cells produced large hypervascular tumors in 100% of mice whereas EpCAM$^-$ cell fractions produced only small and pale-looking tumors in 30% of mice 4 weeks after injection (Figure 5*A* and Supplementary Figure 3*A*; see supplementary material online at www.gastrojournal.org). Similar results were obtained with HuH7 cells (Supplementary Figure 3*B–D*; see supplementary material online at www.gastrojournal.org). As little as 200 EpCAM$^+$ cells could initiate tumors in 8 of 10 injected mice, whereas 200 EpCAM$^-$ cells produced only 1 tumor among 10 injected mice at 6 weeks after transplantation, and the tumor sizes were much larger in the EpCAM$^+$ cells than in the EpCAM$^-$

cells (Figure 5*B* and Supplementary Figure 3*E*; see supplementary material online at www.gastrojournal.org). EpCAM$^+$ cells produced tumors with a mixture of both EpCAM$^+$ and EpCAM$^-$ cells in xenografts, and these cells invaded in the capsule and muscles of the leg adjacent to the tumor (Figure 5*C*). EpCAM$^+$ cells derived from tumors again maintained their tumor-initiating capacity, tumor morphology, and invasive ability in an in vivo serial transplantation experiment (Figure 5*D*). Occasionally, EpCAM$^-$ cell fractions produced a few small tumors that always contained a mixture of EpCAM$^+$ and EpCAM$^-$ cells (data not shown), indicating that the contaminated EpCAM$^+$ cells from FACS sorting contribute to the tumor-initiating ability.

To further validate whether EpCAM$^+$ HCC cells were tumor-initiating cells, we isolated EpCAM$^+$ HCC cells from 2 cases of AFP$^+$ (>600 ng/mL serum AFP) HCC clinical specimens using MACS. Consistently, 1×10^4 EpCAM$^+$ cells could induce tumors in NOD/SCID mice, but up to 1×10^6 EpCAM$^-$ cells failed to do so (Table 1). In addition, similar to HCC cell lines, fresh EpCAM$^+$ tumor cells from 2 clinical HCC specimens were more efficient in forming spheroids in vitro than EpCAM$^-$ cells (Supplementary Figure 4; see supplementary material online at www.gastrojournal.org).

FACS analysis results indicate that a majority of EpCAM$^+$ cells express CD133 in HuH7 cells but not in HuH1 cells (Figure 2*B*), which prompted us to compare the tumorigenic capacity of EpCAM$^+$ and CD133$^+$ cells in these cell lines. Noticeably, EpCAM$^+$ HuH1 cells showed marked tumor-initiating capacity compared with CD133$^+$ HuH1 cells (Figure 5*E* and *F*), whereas EpCAM$^+$ and CD133$^+$ cells had similar tumorigenic ability in HuH7 cells (data not shown).

GSK-3β Inhibition Augments EpCAM$^+$ HCC Cells

To determine the role of Wnt/β-catenin signaling[28] in EpCAM$^+$ HCC cells (Figure 1*B*), we first treated HuH1, HuH7, and HLF cells with a GSK-3β inhibitor BIO (Figure 6*A*), which activates Wnt/β-catenin signaling (Figure 6*B*) and maintains undifferentiation of embryonic stem cells.[38] 6-bromoindirubin-3′-oxime (BIO) increased the EpCAM$^+$ cell population in HuH1 and HuH7 cells when compared with the control methylated BIO (MeBIO) (Figure 6*A*). In contrast, BIO had no effect on the CD90$^+$ cell population, which is more tumorigenic than the CD90$^-$ cell population in HLF (Figure 6*A* and data not shown). Enrichment of EpCAM$^+$ cells was provoked further by the treatment of Wnt10B-conditioned media in HuH7 cells (Figure 6*C*).[34] BIO induced morphologic alteration of HuH7 cells because most cells became small and round when compared with MeBIO and suppressed EpCAM$^-$ AFP$^-$ cell populations (Figure 6*D*). Moreover, BIO induced *TACSTD1*, *MYC*, and *hTERT* expression and spheroid formation (Figure 6*E* and *F*).

Table 1. The Tumor-Initiating Capacity of EpCAM$^+$ Cells From Clinical HCC Specimens

HCC patients				Tumor incidence (mice with tumors/total no. of mice injected)	
No.	% of EpCAM$^+$ HCC cells	Groups	No. of cells injected	2 months	3 months
1	5.2	EpCAM$^+$	1×10^3	0/3	0/3
			1×10^4	2/3	2/3
			1×10^5	2/2	2/2
		EpCAM$^-$	1×10^5	0/3	0/3
			1×10^6	0/2	0/2
2	1.4	EpCAM$^+$	1×10^3	0/2	0/2
			1×10^4	0/1	1/1
		EpCAM$^-$	1×10^4	0/3	0/3
			1×10^5	0/2	0/2

EpCAM Blockage by RNA Interference

One of the hallmarks of CSCs is its resistance to conventional chemotherapeutic agents resulting in tumor relapse and thus targeting CSCs is critical to achieve successful tumor remission. Consistently, 5-FU could increase the EpCAM$^+$ population and spheroid formation of HuH1 and HuH7 cells (Figure 7*A* and *B*) (data not shown), suggesting a differential sensitivity of EpCAM$^+$ and EpCAM$^-$ HCC cells to 5-FU. In contrast, EpCAM blockage via RNA interference dramatically decreased the population of EpCAM$^+$ cells (Figure 7*C*), and significantly inhibited cellular invasion, spheroid formation, and tumorigenicity of HuH1 cells (Figure 7*D–F*). Thus, EpCAM may serve as a molecular target to eliminate HCC cells with stem/progenitor cell features.

Discussion

The cellular origin of HCC is currently in debate. In this study, we found that EpCAM can serve as a marker to enrich HCC cells with tumor-initiating ability and with some stem/progenitor cell traits. EpCAM is expressed in many human cancers with an epithelial origin.[39] During embryogenesis, EpCAM is expressed in fertilized oocytes, embryonic stem cells, and embryoid bodies, suggesting its role in early stage embryogenesis.[40] Furthermore, a recent article indicated that EpCAM is expressed in colonic and breast CSCs.[41] Taken together, these data suggest a critical role of EpCAM in CSCs as well as embryonic and somatic stem cells. Consistently, we found that EpCAM expression is regulated by Wnt/β-catenin signaling[29] and tumorigenic and highly invasive HpSC-HCC is orchestrated by a subset of cells expressing EpCAM and AFP with stem cell–like features and self-renewal and differentiation capabilities regulated by Wnt/β-catenin signaling (this study). Thus, EpCAM may be a common gene expressed in undifferentiated normal cells and HCCs with activated Wnt/β-catenin signaling. It may act as a downstream molecule